A KETOGENIC DIET PROMOTES BLOOD-SPINAL CORD BARRIER RESEALING AND PHENOTYPIC SWITCHING OF PRO-INFLAMMATORY MYELOID CELL INFILTRATES IN A PRECLINICAL MODEL OF MULTIPLE SCLEROSIS.

Kendra S. Plafker[1], Dorothy A. Walton[1], Nathan Pezant[2], and Scott M. Plafker[1,2*]

[1]Aging and Metabolism Research Program and [2]Center for Biomedical Data Sciences
Oklahoma Medical Research Foundation, Oklahoma City, OK USA
[2] Department of Cell Biology, University of Oklahoma Health Sciences Center, Oklahoma City, OK USA

*Corresponding author:
Scott M. Plafker, Aging and Metabolism Research Program, Oklahoma Medical Research Foundation
825 NE 13th St, OKC, OK, 73104.
Email: Scott-Plafker@omrf.org

Keywords
Ketogenic diet, multiple sclerosis, EAE, blood-CNS barrier, phenotypic switching

ABSTRACT

We previously demonstrated that a ketogenic diet (KD) restored vision and motor functions to mice undergoing experimental autoimmune encephalomyelitis (EAE) when administered beginning the day of symptom onset. The follow up studies reported here demonstrate the impacts of the KD on immune cells and immune cell trafficking in this mouse model. The KD dramatically reduced the infiltration of all $CD45^{HI}$ immune cells into the spinal cords of EAE mice when fed for 2 weeks following symptom onset. This reduction was preceded by an increase of myeloid cells in the blood, primarily neutrophils and monocytes/macrophages. One mechanism underlying this altered distribution was accelerated resealing of the blood-SC barrier (BSCB), which initially opened at disease onset to different extents in EAE females and males but was rapidly resealed by the KD in both sexes. This resealing accompanied functional recovery and remarkably occurred whether KD feeding was initiated the day of symptom onset or 6-8 days after symptom onset. Consistent with this resealing, the KD reduced SC levels of secreted IL-1β, the primary cytokine associated with compromising the integrity of CNS-blood barriers. As neutrophils mediate BSCB disruption and were the most markedly reduced infiltrating cell type in response to the KD, we found that the diet reduced SC levels of the neutrophil chemoattractant, CXCL2, and the neutrophil activator IL-6, as well as neutrophil markers of inflammation and pathogenicity. Non-linear dimensionality reduction analyses of our flow cytometry data further revealed that the KD induced phenotypic switching, reducing the frequency of pathogenic myeloid cells in the SC while increasing the frequency of myeloid cells expressing markers associated with resolving inflammation. These studies additionally revealed both common and distinct impacts of the KD on EAE female and male mouse immune cells. Collectively, this work advances a novel mechanistic understanding by which a KD ameliorates autoimmune-mediated MS-like pathologies to promote functional recovery and more broadly, implies that this dietary strategy has potential benefit for healing disrupted blood-CNS barriers and resolving inflammation in multiple neurodegenerative diseases.

INTRODUCTION

MS is the most common neurodegenerative disease in young adults with nearly 3 million individuals afflicted worldwide (1). Experimental autoimmune encephalomyelitis (EAE) mouse models reconstitute hallmark pathologies of MS (2) and have been instrumental in developing disease modifying therapies (DMTs) used to treat people with MS (pwMS) (3). Similar to other autoimmune disorders, MS is more prevalent in females compared to males, with a ≥ 2-fold greater incidence among females (4). This propensity for females has consequently resulted in most EAE studies being performed in female mice (5), yet males with MS can have more severe disability (e.g., (6)), underscoring the need to investigate both sexes using the EAE paradigm to identify common and sex-divergent phenotypes and mechanisms. Furthermore, the immune systems of females and males differ in humans and in mice, and EAE studies comparing sexes have revealed both common and differential immune cell responses (5, 7). Such differences could contribute to the varied DMT efficacies, preferences, and adherences to treatment regimens between the sexes (e.g., (8, 9)), but to date, sufficiently powered studies have not identified sex-based differences in DMT efficacies in humans.

We previously showed that a non-obesogenic ketogenic diet (KD) enriched in fiber, medium chain triglycerides (MCTs; octanoic acid and decanoic acid specifically), and ω-3 fatty acids prevented symptom onset when fed prophylactically to female and male EAE mice. Additionally, the diet restored visual and motor function to both sexes of mice when initiated after symptom onset (10). Small clinical trials involving KDs and low glycemic diets (e.g., the Wahls diet) for pwMS have shown promising outcomes including reduced fatigue, improved quality of life, improved sleep quality, reduced expanded disability status scale (EDSS) scores, reduced levels of serum neurofilament light chain, and improvements in 6-minute walk test and nine-hole peg tests (11-14). However, the mechanisms underlying each of these therapeutic outcomes remain largely unknown.

To identify mechanisms of KD efficacy with respect to how the dietary intervention impacts the immune cell responses in each sex, we performed immune cell profiling studies in the spinal cords (SCs), blood, and bone marrow (BM) of female and male mice undergoing EAE. For all experiments, the KD

was initiated following symptom onset to reflect the timing by which this dietary strategy would likely be leveraged by pwMS in response to symptom flare-ups or by individuals with clinically isolated syndrome that have not received an MS diagnosis and are DMT-naive.

We report here that both females and males had dramatic reductions of total $CD45^{HI}$ infiltrating immune cells in the SC after being fed the KD for 2 weeks with neutrophils being the most reduced (i.e., > 90%). Preceding this reduction, neutrophils and numerous other immune cell types that mediate EAE pathology were elevated in the circulation within a week of diet initiation. Mechanistically, these altered immune cell distributions in the SC and blood indicated that the KD promoted resealing of the blood-spinal cord barrier (BSCB), which we demonstrated experimentally using a fluorescent tracer. Remarkably, this resealing was likewise observed when the diet was initiated a week after symptom onset, and these studies also revealed that EAE females initially had a 2-fold increase in BSCB permeability compared to EAE males. The accelerated BSCB resealing corresponded to a reduction of bioactive IL-1β levels in the CNS. Additional profiling showed that the KD altered surface marker expression on SC-infiltrated neutrophils and monocyte/macrophages consistent with phenotypic switching towards a less pro-inflammatory and more pro-resolution state.

RESULTS

Our previous study using the MOG_{35-55} EAE mouse model of autoimmune-mediated inflammation and demyelination showed that a KD enriched in fiber, MCTs, and omega (ω)-3 fatty acids restored visual and motor function when initiated following symptom onset. The therapeutic efficacy of the diet was comparable in male and female mice (10). The present work applied immune cell profiling to identify mechanistic insights by which the KD mediates therapeutic benefits.

As we previously observed in wild type C57BL/6J mice (10)and repeated here in a reporter strain called 'SMART-Fox' (C57BL/6J background), switching EAE mice to the KD following symptom clinical onset resulted in functional motor recovery beginning within 2 days for females and within 2-4 days for males. This rapid recovery persisted until the termination of experiments at 14 days post-symptom onset (DPSO) (i.e., equal to 14 days of diet administration) (Figs. 1A and 1B, respectively). As detailed in the Material and Methods section, SMART-Fox mice express a reporter for IL-17A expression and enhanced GFP under the endogenous *Foxp3* promoter. Only the GFP reporter was tracked in the present study. KD-mediated motor function recovery corresponded with increased ketones in the circulation at both time points (Fig. 1C) as well as reduced SC lesion sizes and cellularity observed by immunohistochemistry (IHC) (Supplemental Fig. 1).

To circumvent the inherent limitations and variability of quantifying and characterizing infiltrates in tissues using IHC (15, 16), we used multiparameter flow cytometry with validated fluorochrome-labeled monoclonal antibodies (Supplemental Table 1) to profile the immune cell changes mediated by the KD in the SCs, blood, and BM. Tissues were harvested at 5-7 DPSO (aka 'Peak' disease) and at 13-15 DPSO (aka 'Late' disease) (Fig. 1). The surface markers used to define each immune cell type and the abbreviations for all immune cells are compiled in Supplemental Table 2; the flow cytometry gating parameters are provided in Supplemental Fig. 2. Based on KD efficacy in SMART-Fox mice (Fig. 1), all flow cytometry experiments were performed in this strain to facilitate visualizing $FoxP3^+$ Tregs without the need for intracellular transcription factor labeling.

The KD reduces immune cell infiltrate accumulation in the SCs of EAE mice.

Analysis of SCs at Peak disease showed that the KD reduced the abundance of neutrophils in females whereas in males, neutrophils were reduced in some animals but did not reach statistical significance (Fig. 2A). However, in male SCs, the KD significantly reduced Ly6C$^-$ monocytes/macrophages (mono/macs) and microglia (Figs. 2A and 2B, respectively). Diet-mediated fold changes in cell abundances as well as cell types analyzed that did not differ are listed in Table 1, which was constructed from raw cell abundance data provided in Supplemental Table 3.

Consistent with these early neutrophil changes in the SCs of females, ELISA assays of SC extracts at 0, 3, and 6 days post-symptom onset (DPSO) showed that the KD decreased levels of the neutrophil activator, IL-6, in females at 3 DPSO whereas no statistically significant changes were detected in males (Fig. 2C). Likewise, the neutrophil recruitment cytokine CXCL2 was reduced by the KD in females at both 3 and 6 DPSO but not in males (Fig. 2C).

In alignment with motor function recovery after two weeks of diet treatment (Fig. 1), the SCs of females and males at Late disease both had major decreases in the abundance of total CD45$^+$ cells. These reductions were driven largely by the loss of infiltrating CD45$^{\mathbf{HI}}$ immune cells including both CD11b$^+$ myeloid cells and CD11b$^-$ cells (comprised of conventional dendritic cells (cDCs) and all T cells) (Fig. 2D). Similar to Peak disease, males exclusively had reduced numbers of microglia; females trended but did not reach significance (Fig. 2D). We next visualized our multi-dimensional flow cytometry data of SC CD45$^+$ cells at Late disease by T-distributed stochastic neighbor embedding (t-SNE). This analysis showed that the KD led to major reductions in neutrophils, myeloid cells, T helper effector cells (TH), and Tregs in the SCs of both sexes (Fig. 2E). Based on the t-SNE and the central roles of neutrophils, myeloid cells, and T cells in cooperatively driving EAE onset and progression (e.g., (17-23)), we quantified these cell types. In both sexes, the KD decreased infiltrating SC neutrophils by 94% (Fig. 2F and Table 2). We next quantified myeloid subsets distinguished by Ly6C expression. Mono/mac expression of the Ly6C glycoprotein plays an integral role in EAE with higher expression on infiltrating cells associated with pro-inflammatory phenotypes (24) and lower expression associated with tissue repair

(25). The KD differentially decreased Ly6C$^+$ and Ly6C$^-$ mono/macs. Specifically, Ly6C$^+$ mono/macs were reduced by > 80% in both sexes whereas Ly6C$^-$ mono/macs were decreased by 49-60% (Fig. 2F, Table 2). Likewise, the KD decreased SC-infiltrating TH cells and Tregs in both sexes by $\geq$ 70% (Fig. 2G). Quantification of other cell types impacted by the KD (e.g., cDCs, monocyte-derived DCs (moDCs), NKs) showed decreases ranging from 34-86% (Table 2 and Supplemental Table 3).

To determine whether the cell losses within the SC were a consequence of the diet reducing the generation of these cells, we performed parallel immune cell profiling of the blood and BM at Peak (Table 1) and Late disease (Table 2). The blood of KD-fed females at Peak disease showed a trend for *increased* numbers of all CD45$^+$ cells with statistically significant elevations of CD11b$^+$ myeloid cells attributable to elevated neutrophils (Fig. 3A, left graph). Interestingly, the KD exclusively suppressed circulating NK cells in females (Fig. 3A, right graph). In males, the KD increased the numbers of CD45$^+$ cells in the blood at Peak disease, and this was also attributable to elevated neutrophils (Fig. 3A, left graph) along with contributions from CD11b$^+$ myeloid cell populations restricted for Ly6C expression including Ly6C$^-$ CD11c$^+$ cells and moDCs (Fig. 3A, right graph). At Late disease in the blood of females fed the KD, reductions were observed for B cells, NK cells, CD8$^+$ T cells, moDCs, Ly6C$^+$CD11c$^+$ monocytes, and TCRgd cells (Fig. 3B). In contrast, for EAE males the KD sustained increased abundances of circulating CD45$^+$ immune cells at Late disease, with increases in CD11b$^+$ myeloid cells, in particular, neutrophils (Fig. 3B, left graph). Similar to females at Late disease, the KD also decreased NK cells in the blood of males (Fig. 3B, right graph). Additionally, males had decreased cDCs (Fig. 3B, bottom graph).

Profiling of BM at Peak disease revealed that KD-fed female EAE mice had reductions of CD45$^+$ cells distributed across numerous cell types: neutrophils, populations of monocytes such as Ly6C$^+$, Ly6C$^+$ CCR2$^+$, Ly6C$^+$ CD11c$^+$, and moDCs, as well as cDCs and NK cells (Fig. 4A). In contrast, the BM of KD-fed EAE male mice did not have reduced CD45$^+$ cell abundances and only had reductions of Ly6C$^+$ CD11c$^+$ monocytes and TCRgd cells (Fig. 4A). At Late disease, the KD reduced cDCs in the BM of both sexes, and in males additionally suppressed the numbers of B cells, NKs, CD8+ T cells, TH cells, Tregs, and TCRgd cells (Fig. 4B).

Together, these analyses demonstrate that although the KD elicits a few compartment-, time-, and sex-specific differences in immune cell changes in this model, shared responses by EAE females and males to the diet predominate. These include comparable restoration of motor function with similar kinetics (Fig. 1), the wholesale reduction of immune cells in the SC (Table 2), and numerous immunological responses to MOG peptide immunization, consistent with the work of others (5, 7).

To identify immune cell changes elicited by the KD independent of EAE, we fed the KD or CD for 2 weeks to healthy SMART-Fox mice age-matched to the EAE animals. Table 2 shows these data alongside the changes in the blood and BM of EAE mice fed the diets for 2 weeks (i.e., equivalent to the length of feeding in Late disease). A SC comparison is not shown because healthy mice have negligible immune cell infiltrates (i.e., 1,400-4,500 $CD45^{HI}$ cells in healthy SC versus 112,000-415,000 $CD45^{HI}$ cells in EAE mice – Supplemental Table 3). These experiments showed that consumption of the KD reduced the same cell types in the blood of both healthy and Late EAE females, with the exception of B cells being reduced only in EAE mice. In addition, several cell types ($Ly6C^-$ monocytes, $Ly6C^+$ monocytes, moDCs, cDCs) were exclusively reduced in the blood of healthy female mice fed the KD (Table 2). In the blood of healthy KD-fed males, $CD45^+$ cells and $CD11b^+$ cells (including neutrophils) were all comparably increased in abundance in both healthy and Late EAE mice whereas the reduction of NK cells and cDCs occurred only in the context of EAE. Elevated abundances of several additional cell types were observed in the circulation of healthy, KD-fed males including subsets of $Ly6C^-$ and $Ly6C^+$ monocytes as well as moDCs (Table 2). The BM of females with or without EAE each had a single cell type that decreased in abundance (cDCs and $Ly6C^-CD11c^+$ cells, respectively). In male BM however, all the suppressed cell types in EAE mice eating the KD were likewise reduced in the BM of healthy mice except for NK cells. Moreover, healthy KD-fed male BM had increased abundances of $CD45^+$ cells including $CD11b^+$ cells comprised of neutrophils and $Ly6C^+$ monocytes (with and without CCR2 expression) along with reduced numbers of $Ly6C^-CCR2^+$ monocytes. The elevated BM cell populations align with the increases in blood of these same cell types. These data indicate that, *at Late disease,* most

of the immune cell abundance changes in the blood and BM in both sexes during EAE are diet-mediated and not a direct manifestation of the model.

The finding that the KD dramatically reduced immune cell infiltrates in SCs at Late disease (Figs. 2D-G and Table 2) and this reduction was preceded at Peak disease by increased myeloid cells in the blood (Fig. 3A and Table 1) without a corresponding increase in myeloid cell generation in the BM (Fig. 4 and Tables 1, 2), was consistent with the diet resealing the blood-spinal cord barrier (BSCB) to prevent circulating immune cells from entering the inflamed CNS. During EAE, loss of BSCB integrity is required for select immune cell populations to transmigrate from the circulation into the CNS to promote inflammation and disease onset/progression (reviewed in (26)). To directly test the impact of the KD on BSCB integrity and permeability, male and female EAE mice were intraperitoneally injected with a solution of sodium fluorescein (NaFl, molecular weight = 376.3 g/mol) at either 0 DPSO, 3 DPSO, or 6 DPSO with 0 DPSO representing the time at which motor deficits were first observed (i.e., motor score ≥ 1) and mice had not yet been switched from standard chow to the KD or CD. 30 minutes after injection, SCs were collected to quantify extravasated fluorescent tracer (Figs. 5A-B). The amount of NaFl in the serum of each mouse was also quantified to normalize for differences in the volume of tracer injected and/or animal size. These experiments showed that healthy males and females have minimal and comparable BSCB permeability (Figs. 5A and 5B). On the day of motor symptom onset (i.e., 0 DPSO; motor score ≥ 1), the permeability of the BSCB in EAE females was ~2 fold greater than in males (Orange bars, Figs. 5A and 5B; respectively). BSCB permeability peaked at 0 DPSO and was sustained at this level for 3 days in both sexes (Figs. 5A and 5B). Remarkably, by 3 DPSO the KD decreased the permeability of the BSCB in both females and males by ≥ 50% compared to EAE mice fed the CD (Figs. 5A and 5B). By 6 DPSO, males showed a further statistically significant decrease in BSCB permeability. Those fed a KD had BSCB permeability comparable to healthy mice. At this time point, females on both diets had similar permeability, but this permeability was still greater than that of healthy female mice (Fig. 5A). Females fed the CD for 6 days showed significantly decreased BSCB permeability due to the spontaneous resealing that occurs with this model (27); males trended but did not reach statistical

significance. Together, these data show that: (i) the extent of BSCB permeability at motor symptom onset (i.e., 0 DPSO) is sexually divergent (females > males), (ii) the BSCB spontaneously reseals in both sexes between 3 and 6 DPSO as the symptomatic phase of EAE progresses, and (iii) the KD accelerates BSCB resealing in both sexes but to different extents despite improving motor scores comparably (Supplemental Fig. 3).

One potential mechanism underlying the capacity of the KD to accelerate BSCB resealing could derive from reducing SC levels of secreted (i.e., mature) IL-1β. Notably, the mature form of this cytokine is produced by the proteolytic activity of inflammasome-activated caspase-1, an enzyme required for the loss of blood-CNS barrier integrity in the EAE model (28, 29). To test this hypothesis, we generated SC extracts from female and male EAE mice and quantified secreted IL-1β by ELISA at the time points matching the NaFl assays (i.e., 0, 3, and 6 DPSO). In females, the KD reduced IL-1β levels in the SC at both 3 and 6 DPSO (Fig. 5C). In males, IL-1β levels at 6 DPSO were reduced in KD v CD fed mice and at 3 DPSO trended downward for KD-fed mice but did not reach statistical significance although the levels in the KD group (but not the CD group) at this time point were statistically significantly lower compared to 0 DPSO (Fig. 5D). As expected, IL-1β levels at all time points for both sexes and diets were elevated in EAE mice compared to healthy mice (Figs. 5C-D).

To determine if the KD retained efficacy and promoted BSCB resealing when initiated after symptoms had persisted, we repeated the NaFl tracer studies but waited to initiate feeding of the therapeutic diet until 6-8 DPSO. The fluorescent tracer was injected 14-16 days after initiating the KD or CD (i.e., 20-23 DPSO) (Fig. 6A). These studies revealed that the KD retained the capacity to improve motor scores when initiated ~ 1 week after clinical symptom onset, with functional improvements detected within 6 days of treatment for females (Fig. 6B) and 4 days for males (Fig. 6D). Additionally, in both sexes the KD resealed the BSCB compared to the permeability on the day of diet switch (Figs. 6C and 6E). In males, this resealing was additionally statistically significant when compared to CD-fed mice (Fig. 6E) whereas in females, the difference in diet treatments did not reach significance (Fig. 6C).

Neutrophils are an important cell type in MS (21, 27, 30), are essential for EAE onset, but also contribute to EAE progression (20). Our t-SNE analysis showed a striking KD-dependent dropout of neutrophil abundance at Late disease in EAE female and male SCs as well as a retention of select neutrophil subpopulations (Fig. 2E, arrows). To distinguish these retained subpopulations from those neutrophils that were lost and to test the hypothesis that the persistent neutrophil subpopulations have an anti-inflammatory (or naïve) phenotype, we analyzed the differential expression of select surface makers. t-SNE visualization of these data showed that, despite the loss of most neutrophils, those that remained in the SCs of both sexes had relatively reduced expression of Ly6G (Figs. 7A-B lower left panels and Fig. 7C). Ly6G is a glycoprotein that modulates neutrophil migration to sites of inflammation (31), and a decreased median fluorescence intensity (MFI) of Ly6G was identified to be a distinguishing marker of pro-resolution neutrophils in an optic nerve crush model by the Segal laboratory (32). Quantification of SC neutrophil Ly6G MFI by flow cytometry revealed that in both females and males the KD decreased Ly6G expression levels (Fig. 7C), whereas Ly6G MFI was unchanged on neutrophils in the blood (Supplemental Fig. 4) revealing an anatomical compartment-specific effect of the KD in EAE mice. This Ly6G MFI reduction in neutrophils by the KD was additionally detected at Peak disease indicating that it is initiated early, before consistent and dramatic neutrophil loss was observed in males, and then sustained through late disease (Fig. 7C).

The t-SNE plots also indicated that these retained neutrophil subpopulations are likewise enriched for CD62L expression (Figs. 7A-B center panels and Fig. 7D). This adhesion molecule is also known as 'L-selectin' and plays critical roles in the homing and chemotaxis of lymphocytes to lymphoid organs as well as to sites of inflammation and injury (reviewed in (33)). Neutrophils typically shed CD62L upon being activated and as an outcome of transmigration into inflamed tissues (reviewed in (34)), but loss of the marker is not strictly required for such infiltrating activity (e.g., (35)). Thus, the presence of CD62L is associated with naïve homeostatic neutrophils whereas loss of the marker is typically linked to neutrophil activation during inflammation. Using the ratio of $CD62L^{LO}$ to $CD62L^{HI}$ as a proxy for neutrophil activation state with a higher ratio indicating greater activation (e.g., (36)), we found that the

KD dramatically reduced the ratio of CD62L^{LO} to CD62L^{HI} in the SCs of both sexes, consistent with these remaining neutrophils having reduced pathogenicity (Fig. 7D).

Akin to CD62L, the homing receptor CD44 functions in the adhesion of neutrophils to the endothelium and to their subsequent migration out of blood vessels to enter inflamed tissue (37, 38). Further, CD44 can be internalized from the membrane of activated neutrophils and enter the nucleus to modulate azurophilic granules (39). The t-SNE plots showed that the neutrophils remaining in the SC after KD treatment were enriched for surface expression of CD44 in both sexes (Figs. 7A and B, right panels). We verified this by showing that the frequency of neutrophils expressing CD44 on their surface at Late disease in the SCs of females and males treated with the KD increased from 2-5 fold versus those captured from CD-fed mice (Fig. 7E). Together, these data indicate that the neutrophils remaining in the SC at Late disease for mice fed the KD are phenotypically distinct (i.e., Ly6G^{LO}, CD62L^{HI}, CD44^{HI}) from the pro-inflammatory neutrophils (i.e., Ly6G^{HI}, CD62L^{LO}, CD44^{LO}) that drive motor deficits in EAE.

In alignment with KD skewing of the SC milieu towards an anti-inflammatory environment, we next analyzed mono/macs in the SC at Late disease focusing on cell surface expression of Ly6C and CD86. Ly6C on mono/macs is required for CCR2-dependent recruitment to the inflamed CNS but is down-regulated during disease resolution (40, 41). Our analysis revealed that among the CD11b^{+} mono/mac population in the SC at Late disease, the KD decreased Ly6C expression in a process known as phenotypic switching (Fig. 8A) (reviewed in (42)). This enrichment of Ly6C^{-} mono/macs is associated with resolving inflammation (43), in contrast to the pro-inflammatory phenotype in EAE associated with Ly6C^{+} mono/macs (19). Furthermore, CD86 is a co-stimulatory protein that functions in antigen presentation to reactivate T cells (44), and the KD reduced the proportion of pro-inflammatory mono/macs (i.e., CD86^{+}Ly6C^{+}) in both sexes with concomitant increases in anti-inflammatory (CD86^{+} Ly6C^{-}), naïve (CD86^{-}Ly6C^{+}), and tissue repair (CD86^{-}Ly6C^{-}) mono/macs (Fig. 8B). Together, these surface marker data provide additional evidence that the KD induces phenotypic switching in myeloid cell populations (e.g., neutrophils, mono/macs) to skew the balance in the CNS of EAE mice in favor of resolving inflammation and promoting tissue repair/recovery.

DISCUSSION

Pilot trials for pwMS have shown promising therapeutic efficacy for KDs with demonstrated improvements in fatigue and depression, expanded disability status scale (EDSS) scores, 6-minute walk, 9-hole peg test scores (13), and sleep quality (14). 3 months post-trial the positive impacts of the KD were largely sustained, and individuals for whom the KD led to the greatest reductions in body mass and fatigue were the most likely to maintain a low-carbohydrate dietary regimen post-trial (45). In this same study, higher levels of serum β-HB correlated with greater decreases in serum Nfl (sNfl) levels, a marker of axonal breakdown, compared to pre-trial levels (46). An independent trial also showed a reduction in sNfl levels after 6 months (11). In other studies, 4 months of a KD improved lean muscle mass and reduced markers of inflammation and oxidation (47) whereas an adapted KD restricted expression of several enzymes that mediate the biosynthesis of pro-inflammatory eicosanoids (48).

The therapeutic efficacy of KDs has been investigated in rodent EAE studies with improvements demonstrated for motor functions and vision as well as spatial learning and memory (10, 49-51). These improvements were accompanied by reductions of pro-inflammatory cytokines and chemokines (10, 50, 51). Our previous study reported that a KD enriched in fiber, MCTs, and ω-3 fatty acids could prevent or severely delay the onset and severity of both motor and visual deficits when fed to EAE mice prior to immunization. Additionally, the diet restored visual and motor function when initiated coincident with symptom onset (10).

The findings reported here advance the field in several ways. First, we discovered that the KD accelerated the kinetics of BSCB resealing (Figs. 5 and 6). Underlying this effect was the reduced secretion in the SC of IL-1β, the primary cytokine driving loss of BSCB integrity (52, 53). Remarkably, the KD accelerated BSCB resealing whether feeding was initiated the day of symptom onset or 6-8 days after symptom onset. For both treatment regimens, the diet began restoring motor functions within a few days in both sexes, indicating the potential to leverage this dietary strategy to mitigate symptoms in response to acute relapses for pwMS and for treatment-naïve individuals experiencing clinically isolated syndrome prior to an MS diagnosis. Second, we found in both sexes that 2 weeks of the KD robustly decreased the

abundance of total SC infiltrates and critically, induced phenotypic switching to anti-inflammatory and naïve phenotypes within the subpopulations of neutrophils and mono/macs that remained in the SC (Figs. 7 and 8, respectively). Third, in contrast to the efficacy of the KD to restore motor function comparably in EAE females and males (Fig. 1), the diet impacted immune cell abundances in the blood and BM differently between sexes (e.g., Figs. 3, 4, and Tables 1 and 2).

Our data and others support that the restoring of BSCB integrity by the KD stems from the diet inhibiting the NLRP3 inflammasome and/or inhibiting signaling upstream of inflammasome activation (e.g., P2X7 receptor activity (54, 55)). In EAE, neutrophil transmigration into the CNS parenchyma is accompanied by an amplification of inflammasome activity and IL-1β secretion that drives BSCB loss of integrity (28). In alignment with this hypothesis, our data show that the KD reduces IL-1β levels in SCs (Figs. 5C-D). Thus, by reducing neutrophil infiltration into the SC of EAE mice and/or by limiting inflammasome activation in neutrophils (Figs. 2A and 2F), the KD limits a primary source of IL-1β production in the CNS to restrict BSCB permeability. Additional mechanistic contributions could come from the elevated β-HB generated by the KD (Fig. 1C). This ketone body is an agonist of the hydroxycarboxylic acid receptor 2 (HCA_2R), and multiple lines of evidence show that HCA_2R activation inhibits NF-κB signaling upstream of the NLRP3 inflammasome (56-58) and restricts neutrophils from accumulating in the CNS (59). Another mechanism could involve infiltrating mono/macs expressing HCA_2R but with reduced or absent expression of Ly6C. In a murine ischemic stroke model, this cell population mediated the efficacy of the HCA_2R agonist nicotinic acid (60). Future studies using genetic and pharmacological manipulation of HCA_2R will reveal the relative contribution of this pleiotropic receptor to KD efficacy.

Independent of HCA_2R, β-HB could also promote BSCB resealing by (i) increasing the expression of the mRNAs of several tight junction proteins among the endothelial cells that comprise the BSCB/BBB, and/or (ii) reducing the expression of matrix metalloproteinases (MMPs), like MMP-9, that degrade CNS-blood barriers (e.g., (61, 62)). These actions of β-HB stem from the ketone body inhibiting histone deacetylase 3 (HDAC3) (63, 64), and HDAC inhibition can decrease inflammasome activation (65).

Neutrophils were the earliest and most sustainably impacted cell type in response to the KD. These granulocytes have been underappreciated in MS due to their limited detection in mature lesions, but compelling evidence implicates them in the acute stages of lesion formation in both MS and EAE (27). Further, neutrophils are elevated and primed in the blood and cerebral spinal fluid during MS relapses (21, 30), and administration of the neutrophil recruitment factor G-CSF severely exacerbated disease in some pwMS (66). The KD significantly reduced neutrophil abundance in female SCs after only a few days of diet treatment (Fig. 2A) and dramatically decreased neutrophils (i.e., by > 90%) in the SCs of both sexes at Late disease (Fig. 2F). These reductions fit with the central role that neutrophils, in conjunction with microglial cells, astrocytes, and endothelial cells, play in mediating blood-CNS barrier breakdown in EAE (27, 67-69) and other models of CNS injury including those using lipopolysaccharide (69, 70). Moreover, the robust depletion of neutrophils by the KD in females at Peak disease coincided with reductions in SC levels of IL-6 and the neutrophil chemoattractant CXCL2, which function cooperatively in recruiting neutrophils to sites of inflammation (Fig. 2C). Among the neutrophils that persisted in the CNS, the KD polarized (i.e., phenotypically switched) these cells towards an anti-inflammatory and pro-resolution phenotype that was evident at both Peak and Late for females but only at Late disease for males (Fig. 7).

The mechanisms underlying the KD-mediated phenotypic switching of multiple myeloid cell populations (Figs. 7 and 8) may relate to the reliance of these cell types on metabolic reprogramming that favors glycolysis for their activation, expansion, and eventual pathogenicity (reviewed in (40, 71)). For neutrophils, restricting glycolysis within the hypoxic environment of inflamed tissues can increase apoptosis (72), and this cell autonomous effect was confirmed by culturing neutrophils in limited glucose (73). The severe limitation of dietary glucose by the KD may therefore be sufficient to amplify neutrophil apoptosis at sites of inflammation within the CNS. Additionally, as mentioned above, KDs can inhibit NLRP3 inflammasome activity (55, 74-77), and this activity within neutrophils is specifically required for BBB breakdown and the subsequent migration of these cells into the inflamed CNS of EAE mice (78). Importantly, an amelioration of neutrophil NLRP3 inflammasome activity by the KD is consistent with

our data showing reduced levels of secreted IL-1β (Figs. 5C-D) at the critical time points in the disease course when neutrophils are the primary source of this cytokine (27).

For mono/macs, the KD promoted phenotypic switching in favor of non-classical (i.e., pro-resolution) macrophages (Ly6C$^-$) through dramatically reducing classical inflammatory (i.e., pro-inflammatory) (Ly6C$^+$) macrophages (Fig. 8). In addition, the KD reduced the remaining fraction of Ly6C$^+$ cells that co-expressed high expression levels of CD86 in both sexes (Fig. 8B), consistent with promoting a more naïve phenotype. Notably, a bioenergetic shift underlies the phenotypic switching of monocytes from Ly6C$^+$ to Ly6C$^-$ that fits with the very low carbohydrate content of the KD. Specifically, Ly6C$^+$ monocytes rely on enhanced glycolysis mediated by IL-17 and GM-CSF driven upregulation of glucose transporters to import more glucose (79) whereas a switch of Ly6C$^+$ monocytes favoring oxidative phosphorylation promotes conversion to non-classical Ly6C$^-$ mono/macs that promote resolution at sites of inflammation (80). Notably, this reduction of Ly6C$^+$ mono/macs and phenotypic switching of the remaining mono/macs from pro-inflammatory to anti-inflammatory or naïve has also been observed for pharmacological and genetic strategies that mitigate EAE and other murine models of CNS demyelination (e.g., (81)). For example, reductions of Ly6C$^+$ monocytes leading to ameliorated EAE have been reported for nucleotide-oligomerization domain 2 (NOD2) agonists (81), C-C chemokine receptor 4 (CCR4) knockout mice (82), and IL-17 knockout mice (83). Future studies to determine if the KD shares mechanisms of efficacy with the above will provide additional insights into this dietary intervention. Collectively, our findings along with those in the literature support that dietary carbohydrate restriction could provide a relatively safe, rapid, and reversible means of tempering myeloid cell pathogenicity during autoimmune flare-ups.

Our flow cytometry analyses of SC, blood, and BM showed that the KD differentially impacted the immune cell profiles of female and male EAE mice only modestly in the SC, but more extensively in the blood and BM (Figs. 3 and 4, respectively). Although the implications of these sex differences in peripheral immune cells remain to be determined, their collective impact appears to be relatively minor as the KD: (a) restored motor deficits comparably in the sexes (Fig. 1), (b) promoted BSCB resealing to near

comparable extents (Figs. 5 and 6), (c) severely reduced the abundance of myeloid and T cell infiltrates in the CNS of both sexes (Table 2), and (d) induced phenotypic switching of neutrophils and mono/macs in the SC of both sexes.

In summary, this work advances novel mechanisms by which a KD mitigates autoimmune-mediated MS-like pathologies to promote functional recovery (Fig. 9). These findings provide a plausible unifying explanation for the beneficial impacts of KDs across a range of CNS diseases involving disrupted blood-CNS barriers and myeloid cell-mediated pathogenicity including MS, drug-resistant epilepsy, ALS, AD, PD, and schizophrenia (e.g., (11, 14, 84-88)).

MATERIALS AND METHODS

EAE procedure and mice

7.5-13 week old mice were immunized with 250 ug of a peptide corresponding to amino acids 35-55 of murine MOG emulsified in incomplete Freund's adjuvant supplemented with 250 ug heat-inactivated *Mycobacterium tuberculosis* (Thermo Fisher Scientific; DF3114338). 250 ng of *Bordetella pertussis* toxin is administered the day of immunization and again 2 days later. Clinical symptoms begin 11-16 days post-immunization. Mice are weighed daily and scored daily for motor deficits using our published scoring system (10). Wild type C57BL/6J mice were used for experiments involving IHC, sodium fluorescein and ELISAs. A transgenic C57BL/6J strain we call 'SMART-Fox' was used for flow cytometry experiments to circumvent the need for intracellular staining. SMART-Fox mice were generated by crossing Smart-17A mice (JAX stock # 032406;) to B6-Foxp3^{EGFP} mice (JAX stock # 006772) and are homozygous for each reporter construct. Males are hemizygous for the Foxp3-GFP transgene because this construct is on the X chromosome. SMART-Fox mice express a non-signaling form of the human nerve growth factor receptor upon activation of the IL-17A locus. The B6-Foxp3^{EGFP} transgene co-expresses enhanced GFP and Foxp3 under the endogenous *Foxp3* promoter with GFP expression accurately marking the Foxp3^{+} CD4^{+} Treg population. Notably, the two parental strains have been validated in the MOG$_{35\text{-}55}$-EAE model (89, 90). Importantly, we observe comparable motor deficits between SMART-Fox mice and wild type C57BL/6J mice. Blood ketones were measured using Precision Xtra Blood Ketone Monitoring System.

Diet compositions

Teklad control (TD.170645) and ketogenic (TD.10911) diets were obtained from Envigo, Inc. The ketogenic diet provides 4.7 Kcal/g with 22.4% Kcal from protein, 0.5% Kcal from carbohydrate, and 77.1% Kcal from fat. The control diet provides 3.6 Kcal/g with 20.4% Kcal from protein, 69.3% Kcal from carbohydrate, and 10.4% Kcal from fat. Diet ingredients are provided in our previous publication (10). Food and water (containing 2.6 ml/L electrolytes, Electrolyte drops; KetoChow) were provided *ad*

libitum and additional hydration/electrolytes were provided to animals showing signs of dehydration using intraperitoneal saline injections.

Intervention Diet studies

Unless otherwise indicated, all studies in this manuscript used an intervention paradigm in which the animals are maintained on standard chow until being switched to either the CD or KD at motor symptom onset and then maintained on diet for the indicated times.

Therapeutic Diet study

In the therapeutic paradigm used exclusively for Fig. 6, mice were maintained on standard chow until 6-8 days post motor symptom onset. At that time, only mice that had reached a motor score of at least 2.5 within the first 6-8 days were switched to CD or KD for 2 additional weeks before harvest.

Multiparameter Flow cytometry

At the indicated times, animals were sacrificed by CO_2 asphyxiation, blood was collected by cardiac puncture followed by perfusion with PBS and decapitation. RBCs were lysed in 100ul blood, remaining cells were washed and stained. Bone marrow was flushed from one leg (femur + tibia) per mouse, RBCs were lysed and 5 million cells were stained. Spinal cords were dissected, dissociated mechanically and incubated in collagenase and DNase. Cells were filtered through a 40uM mesh filter, washed with PBS and myelin was removed using a 40% Percoll gradient; all remaining spinal cord cells were stained. Cells were incubated with BD Horizon Fixable Viability Stain 450 and anti-CD16/32 for Fc block. Supplemental Table 1 lists all the fluorophore-conjugated surface staining antibodies used. Finally, cells were collected on a Cytek Aurora 5 laser instrument and analyzed using FlowJo v 10.

IHC

Fixed, paraffin-embedded spinal cord sections were de-paraffinized, heated in antigen retrieval citrate buffer in a Retriever 2100 (Aptum Biologics) and then incubated with anti-proteolipid protein (α-PLP) (rat: 1:200 dilution; Millipore, Inc.). Nuclei were counterstained with Hoechst, and images were captured using a Zeiss Axioscan 7 digital slide scanner housed in the OMRF Imaging Core.

Sodium fluorescein assay

EAE mice were intraperitoneally injected with 100ul 10% sodium fluorescein (NaFl) at either 0 DPSO, 3 DPSO, or 6 DPSO (Fig. 5) or at 21 DPSO (Fig 6). 30 minutes post-injection, spinal cords and blood were collected to quantify extravasated fluorescent tracer and serum concentrations, respectively. NaFl was quantified using a SpectraMax M2 plate reader (Molecular Devices).

ELISAs

Spinal cords were collected, snap frozen in liquid nitrogen and stored at -80ºC to simultaneously measure cytokines from all time points and experiments. Spinal cords were weighed, thawed and mechanically dissociated in PBS containing EZBlock protease inhibitor cocktail (Biovision). The analytes measured were IL-6 (Invitrogen, cat#5017218), IL-1β (Invitrogen, cat# 887013A22), and CXCL2 (R&D, MM200) using a SpectraMax M2 plate reader (Molecular Devices).

Statistical Analyses

All graphs show average of all data points per sex and treatment with error bars indicating standard error of the mean. Two-tailed, unpaired Student's t test was used unless a non-normal distribution was seen by Shapiro-Wilk test in which case, Mann-Whitney U test was used.

ACKNOWLEDGEMENTS

This work was supported in part by grant R01EY033782 from the National Eye Institute of the National Institutes of Health. The content is solely the responsibility of the authors and does not necessarily represent the official views of the National Institutes of Health. We thank Dr. Robert Axtel for informed discussions and Dr. Susan Kovats for help with data interpretation and for manuscript edits and suggestions. We also extend thanks to Tamy Aguero-Fraire for technical assistance, and to Dr. Katarzyna Zyla-Jackson for help with harvesting female spinal cords. We also thank Dr. Caleb Marlin for the Axioscan analysis; the instrument was purchased by the ACI program at OMRF.

AUTHOR CONTRIBUTIONS

KSP: experimental design, acquisition and analysis of data, writing, editing. DAW: acquisition and analysis of data, editing. NP: model design from data analysis. SMP: experimental design, data analysis, writing, and editing.

DATA AVAILABILITY

The data generated and analyzed for this study are all included in this published article and its Supplementary information files.

COMPETING INTERESTS STATEMENT

The authors declare no competing interests.

FIGURE LEGENDS

Tables 1 and 2. Immune cell profiling of SCs, blood, and BM. Tissues were harvested from EAE mice at Peak (Table 1) or Late (Table 2) disease. Immune cell profiling was done by multiparameter flow cytometry using validated fluorochrome-labeled monoclonal antibodies. Tables list fold change of KD compared to CD. Only cell types that reached statistical significance are assigned fold change. Blank cells indicate that statistical significance was not reached for that cell type. Heatmaps show **green** entries representing fold decreased cell abundance for KD and **red** entries representing fold increased cell abundance for KD. The raw data to generate both tables is provided in Supplemental Table 3.

Figure 1. The KD restores motor functions to female and male mice undergoing EAE. SMART-Fox mice immunized with MOG_{35-55} were fed either KD or CD following symptom onset (motor score ≥ 1) and maintained on their respective diets for 14 days unless indicated otherwise. Motor scores were tracked daily for females (**A**) and males (**B**). n=15-17 mice/sex/diet. 'Peak' disease represents 5-7 days post-symptom onset (DPSO) and 'Late' disease represents 13-15 DPSO, the two time points when tissues were harvested for the subsequent figures. (**C**) Blood ketone levels (mmol/L) measured at Peak and Late disease. The number of mice used for measurements is indicated on the data bars. Sexes and diets are indicated using the following abbreviations: female mice on CD (FCD), female mice on KD (FKD), male mice on CD (MCD), and male mice on KD (MKD). These abbreviations are used throughout for labeling figures. Asterisks denote statistical significance ($p<0.05$) as determined by two-tailed, unpaired Student's t test.

Figure 2. The KD reduces the cell types that mediate EAE pathogenicity in the SCs of female and male mice. (A) Representative flow cytometry pseudo-colored density plots gated on Ly6C and Ly6G expression of the $CD45^{HI}$ immune cells recovered from SCs at Peak disease. Sexes and diets are indicated across the top. Left graph shows average number of neutrophils and right graph shows average number of $Ly6C^{-}$ mono/macs in SC at Peak disease as a function of diet. Each open circle on graph represents an

individual animal, and the coloring of graph labels is matched to the boxes in the flow diagrams from which cell numbers were derived. (**B**) Same as (A) with gating on CD45 and CD11b expression to label microglia, marked in red polygons. The accompanying graph shows average microglial cell number and data from individual animals. (**C**) Graphs of lL-6 and CXCL2 quantified from SC extracts as a function of sex, diet, and DPSO (equivalent to the # of days mice were fed KD or CD). Left graphs are female data, and right graphs are male data. n=5-13 mice/sex/treatment. (**D**) Representative flow cytometry pseudo-colored density plots of SC immune cells at Late disease gated on CD45 and CD11b expression. $CD45^{HI}$ cells comprised of $CD45^{Hi}$ $CD11b^{-}$ and $CD45^{Hi}$ $CD11b^{+}$ cells, marked in blue and pink polygons, respectively. Total $CD45^{+}$ cells comprised of $CD45^{HI}$ cells plus microglia (marked in red polygon). Graphs show abundances of the indicated cell types as a function of diet and sex. (**E**) t-SNE plots generated from flow cytometry data of Late Disease SC immune cell profiling. Female plots are to the left of the key and male plots are to the right. Top plots (adjacent to key) are composites of CD and KD plots. Below each composite is the plot for CD on the left and KD on the right. Cell populations are color coded in all plots as defined in the key. Black arrows mark retained neutrophil populations. Data for t-SNE analysis from n=3 mice/sex/diet. (**F, G**) Representative flow cytometry plots generated from SC $CD45^{HI}$ $CD11b^{+}$ cells isolated at the Late time point. In (**F**), cells gated on Ly6C and Ly6G expression giving rise to graphs of neutrophils, $Ly6C^{+}$ mono/macs, and $Ly6C^{-}$ mono/macs abundances. In (**G**), cells gated on CD4 and FoxP3 expression (i.e., GFP) giving rise to graphs of T helper cell and T regulatory cell (Treg) abundances as a function of diet. n=9-13 mice/sex/diet. In all graphs, asterisks denote statistical significance * $p<0.05$ as determined by Mann-Whitney U test.

Figure 3. The KD increases multiple immune cell populations in the circulation. (A,B) Graphs depicting the abundances of different cell types that changed at Peak disease (**A**) or Late disease (**B**) in the blood as a function of sex and diet. Graphs were constructed from flow cytometry data, and all cell types profiled (including those that did not change) are provided in Supplemental Table 3. n=9-13

mice/sex/diet. Asterisks denote statistical significance * $p<0.05$ as determined by two-tailed, unpaired Student's t test.

Figure 4. The KD differentially impacts multiple immune cell populations in the bone marrow (BM). (A, B) Graphs depicting the abundance of cell types that changed at Peak disease (**A**) or Late disease (**B**) in the BM as a function of sex and diet. All graphs were constructed from flow cytometry data, with all cell types profiled shown in Supplemental Table 3. n=9-13 mice/sex/diet. Asterisks denote statistical significance * $p<0.05$ as determined by two-tailed, unpaired Student's t test.

Figure 5. The KD accelerates resealing of the BSCB. (A, B) Graphs of extravasated sodium fluorescein (NaFl) isolated from SC extracts at the indicated times DPSO. NaFl is expressed on the y-axis as the ratio of the fluorescent tracer in the SC relative to the amount in the serum. Each open circle represents an individual animal. "Healthy" are age- and sex-matched non-EAE mice. n=4-13 mice/sex/diet. (**C**, **D**) Graphs of ELISA data quantifying secreted lL-1β in SC extracts as a function of sex, diet, and DPSO (equivalent to the # of days mice fed KD or CD). Secreted lL-1β was recovered from mice at 0 DPSO, 3 DPSO, and 6 DPSO. n=5-13 mice/sex/diet. Statistical significance * $p<0.05$ as determined by Mann-Whitney U test. For (**A-D**), asterisks denote statistical significance * $p<0.05$ vs CD; # indicates $p<0.05$ vs Healthy; **$** indicates $p<0.05$ vs 0 DPSO; and • indicates $p<0.05$ vs Female.

Figure 6. The KD improves motor function and reseals the BSCB when initiated 1 week after clinical symptom onset. (A) Schematic of study design to test if the KD could promote BSCB resealing and improve motor function when initiated 6-8 DPSO. **(B, D)** Graphs of motor score changes each day compared to the motor score on the day of diet switch (i.e., 6-8 DPSO) for females (B) and males (D); n=10-13 mice/sex/diet. **(C, E)** Graphs of extravasated NaFl expressed as a ratio of the tracer in the SC relative to the serum for EAE females (C) and EAE males (E). Open circles represent individual animals. n=10-13 mice/sex/diet. 6 DPSO data derived from Fig. 5A and 5B is provided for comparison to highlight

the capacity of the KD to further reduce BSCB permeability beyond the spontaneous resealing observed at 6 DPSO. Asterisks denote statistical significance ($p < 0.05$) between CD and KD treatment for 14 days. # denotes statistical significance ($p < 0.05$) compared to data from 0 days post diet switch.

Figure 7. The KD reduces total neutrophil abundance in the SCs of EAE mice but preserves subpopulations expressing surface markers associated with inflammation resolution. (A, B) Top row t-SNE visualization of total neutrophils in the SCs of female (A) and male (B) EAE mice treated with CD or KD and harvested at Late disease. The 12 smaller t-SNE plots show intensity of labeling of neutrophils for the indicated cell surface markers. Heat map indicates HI (red) and LO (blue) intensity(**C**) Histogram and graphs of Ly6G median fluorescence intensity (MFI) on SC neutrophils as a function of sex, diet, and time of disease course. (**D**) Histogram of CD62L MFI and graphs of SC neutrophil activation states represented by the ratio of $CD62L^{LO}$ to $CD62L^{HI}$ expression determined by flow cytometry. (**E**) Histogram and graphs of CD44 MFI on SC neutrophils. Asterisks in all graphs denote statistical significance *$p<0.05$ as determined by two-tailed, unpaired Student's t test or alternatively, by Mann-Whitney U test if Shapiro-Wilk test for normality showed a non-normal distribution. Data for females shown in left graphs and for males in right graphs.

Figure 8. The KD promotes phenotypic switching of spinal cord mono/macs favoring an anti-inflammatory environment. (A) Histogram and graph showing KD-mediated reductions in the percentage of total mono/macs that are $Ly6C^{+}$ in the SC at Late disease for both sexes. **(B)** Representative flow cytometry plots of mono/macs stained for CD86 and Ly6C. The left 4 quadrants show pseudo-colored density plots of compiled data along with phenotype descriptions based on the expression levels of both markers. The right and center 4 quadrants show representative distributions of cells for females (center) and males (right) with blue color marking cells from animals fed CD and red color marking cells from animals fed KD. The accompanying graph shows the frequency of mono/macs in SCs at Late disease based on CD86 and Ly6C expression and the corresponding phenotype associated with the presence or

absence of these two markers. Circles represent individual animals. Asterisks in all graphs denote statistical significance *p<0.05 vs CD as determined by two-tailed, unpaired Student's t test.

Figure 9. Model of the impacts of the KD on immune cells and the BBB. Our data support that the KD restores motor function to symptomatic EAE mice by several mechanisms. The diet: (1) accelerates resealing of the BBB (i.e., blood-CNS barriers) to limit the accumulation of neutrophils and monocytes in the CNS, (2) limits T cell accumulation in the CNS, (3) reduces cytokines in the SC that drive the loss of BBB integrity (IL-1β) and recruit neutrophils to sites inflammation (IL-6 and CXCL2), and (4) induces phenotypic switching of myeloid cells to promote inflammation resolution. Blue ellipses represent pro-resolution (anti-inflammatory) cells and red stars mark pro-inflammatory cells. BBB = blood-CNS barrier. Different colored dots represent the indicated cytokines.

Supplemental Figure 1. The KD reduces lesion size and cellularity in the spinal cords of EAE mice. Spinal cords were harvested at the Late time point and processed for IHC with anti-PLP (the main protein component of myelin) to mark myelin loss and with Hoechst to mark cellularity as a read-out of cellular infiltrates. Insets show lesion outline (PLP) and extent of cellularity (Hoechst).

Supplemental Figure 2. Flow cytometry gating strategies. Gating strategy used on cells for immune cell profiling. SC gating strategy shown on top; blood and BM strategy shown on the bottom.

Supplemental Figure 3. The KD improves motor function comparably in both sexes.
Graph of EAE motor scores for mice used in the NaFl studies shown in Fig 5. Asterisks denote statistical significance *p<0.05 as determined by two-tailed, unpaired Student's t test.

Supplemental Figure 4. The KD does not change the Ly6G MFI of circulating neutrophils. Graphs of Ly6G MFI within circulating neutrophils as a function of sex, diet, and time of disease course. n=9-13 mice/sex/diet. ns = not statistically significant.

Supplement Table 1: List of fluorochrome-labeled antibodies, companies, and catalog numbers used for flow cytometry studies.

Supplemental Table 2. Name, abbreviation and flow cytometry surface markers used to identify each immune cell type analyzed.

Supplemental Table 3. Immune cell profiling raw data for SC, blood, and BM. Data provided for EAE mice harvested at Peak and Late. Data for healthy (non-EAE) age- and sex-matched mice fed the KD or CD for two weeks is also provided. Statistically significant differences (* $p<0.05$) determined by two-tailed, unpaired Student's t test for blood and BM or by Mann-Whitney U test for SC are bolded. Heatmap colors highlight the scale of the differences.

REFERENCES

1. Walton C, King R, Rechtman L, Kaye W, Leray E, Marrie RA, et al. Rising prevalence of multiple sclerosis worldwide: Insights from the Atlas of MS, third edition. Multiple sclerosis. 2020;26(14):1816-21.
2. Glatigny S, Bettelli E. Experimental Autoimmune Encephalomyelitis (EAE) as Animal Models of Multiple Sclerosis (MS). Cold Spring Harb Perspect Med. 2018;8(11).
3. Constantinescu CS, Farooqi N, O'Brien K, Gran B. Experimental autoimmune encephalomyelitis (EAE) as a model for multiple sclerosis (MS). Br J Pharmacol. 2011;164(4):1079-106.
4. Sellner J, Kraus J, Awad A, Milo R, Hemmer B, Stuve O. The increasing incidence and prevalence of female multiple sclerosis--a critical analysis of potential environmental factors. Autoimmun Rev. 2011;10(8):495-502.
5. Wiedrick J, Meza-Romero R, Gerstner G, Seifert H, Chaudhary P, Headrick A, et al. Sex differences in EAE reveal common and distinct cellular and molecular components. Cell Immunol. 2021;359:104242.
6. Golden LC, Voskuhl R. The importance of studying sex differences in disease: The example of multiple sclerosis. J Neurosci Res. 2017;95(1-2):633-43.
7. Lasrado N, Jia T, Massilamany C, Franco R, Illes Z, Reddy J. Mechanisms of sex hormones in autoimmunity: focus on EAE. Biol Sex Differ. 2020;11(1):50.
8. Hegen H, Berek K, Deisenhammer F, Berger T, Enzinger C, Guger M, et al. Sex impacts treatment decisions in multiple sclerosis. Journal of neurology. 2024;271(6):3256-67.
9. Higuera L, Carlin CS, Anderson S. Adherence to Disease-Modifying Therapies for Multiple Sclerosis. J Manag Care Spec Pharm. 2016;22(12):1394-401.
10. Zyla-Jackson K, Walton DA, Plafker KS, Kovats S, Georgescu C, Brush RS, et al. Dietary protection against the visual and motor deficits induced by experimental autoimmune encephalomyelitis. Frontiers in neurology. 2023;14:1113954.
11. Bock M, Steffen F, Zipp F, Bittner S. Impact of Dietary Intervention on Serum Neurofilament Light Chain in Multiple Sclerosis. Neurology(R) neuroimmunology & neuroinflammation. 2022;9(1).
12. Brenton JN, Banwell B, Bergqvist AGC, Lehner-Gulotta D, Gampper L, Leytham E, et al. Pilot study of a ketogenic diet in relapsing-remitting MS. Neurology(R) neuroimmunology & neuroinflammation. 2019;6(4):e565.
13. Brenton JN, Lehner-Gulotta D, Woolbright E, Banwell B, Bergqvist AGC, Chen S, et al. Phase II study of ketogenic diets in relapsing multiple sclerosis: safety, tolerability and potential clinical benefits. J Neurol Neurosurg Psychiatry. 2022;93(6):637-44.
14. Perlman J, Wetmore E, Lehner-Gulotta D, Banwell B, Bergqvist AGC, Coleman R, et al. Impact of a ketogenic diet on sleep quality in people with relapsing multiple sclerosis. Sleep Med. 2024;122:213-20.
15. Mebratie DY, Dagnaw GG. Review of immunohistochemistry techniques: Applications, current status, and future perspectives. Semin Diagn Pathol. 2024;41(3):154-60.
16. Taylor CR, Levenson RM. Quantification of immunohistochemistry--issues concerning methods, utility and semiquantitative assessment II. Histopathology. 2006;49(4):411-24.
17. Croxford AL, Lanzinger M, Hartmann FJ, Schreiner B, Mair F, Pelczar P, et al. The Cytokine GM-CSF Drives the Inflammatory Signature of CCR2+ Monocytes and Licenses Autoimmunity. Immunity. 2015;43(3):502-14.
18. Fletcher JM, Lalor SJ, Sweeney CM, Tubridy N, Mills KH. T cells in multiple sclerosis and experimental autoimmune encephalomyelitis. Clinical and experimental immunology. 2010;162(1):1-11.
19. King IL, Dickendesher TL, Segal BM. Circulating Ly-6C+ myeloid precursors migrate to the CNS and play a pathogenic role during autoimmune demyelinating disease. Blood. 2009;113(14):3190-7.
20. Pierson ER, Wagner CA, Goverman JM. The contribution of neutrophils to CNS autoimmunity. Clinical immunology. 2018;189:23-8.
21. Rumble JM, Huber AK, Krishnamoorthy G, Srinivasan A, Giles DA, Zhang X, et al. Neutrophil-related factors as biomarkers in EAE and MS. J Exp Med. 2015;212(1):23-35.
22. Shaked I, Hanna RN, Shaked H, Chodaczek G, Nowyhed HN, Tweet G, et al. Transcription factor Nr4a1 couples sympathetic and inflammatory cues in CNS-recruited macrophages to limit neuroinflammation. Nature immunology. 2015;16(12):1228-34.

23. Van Kaer L, Postoak JL, Wang C, Yang G, Wu L. Innate, innate-like and adaptive lymphocytes in the pathogenesis of MS and EAE. Cell Mol Immunol. 2019;16(6):531-9.
24. Li YH, Zhang Y, Pan G, Xiang LX, Luo DC, Shao JZ. Occurrences and Functions of Ly6C(hi) and Ly6C(lo) Macrophages in Health and Disease. Front Immunol. 2022;13:901672.
25. Shechter R, Miller O, Yovel G, Rosenzweig N, London A, Ruckh J, et al. Recruitment of beneficial M2 macrophages to injured spinal cord is orchestrated by remote brain choroid plexus. Immunity. 2013;38(3):555-69.
26. Sweeney MD, Sagare AP, Zlokovic BV. Blood-brain barrier breakdown in Alzheimer disease and other neurodegenerative disorders. Nature reviews Neurology. 2018;14(3):133-50.
27. Aube B, Levesque SA, Pare A, Chamma E, Kebir H, Gorina R, et al. Neutrophils mediate blood-spinal cord barrier disruption in demyelinating neuroinflammatory diseases. J Immunol. 2014;193(5):2438-54.
28. Levesque SA, Pare A, Mailhot B, Bellver-Landete V, Kebir H, Lecuyer MA, et al. Myeloid cell transmigration across the CNS vasculature triggers IL-1beta-driven neuroinflammation during autoimmune encephalomyelitis in mice. J Exp Med. 2016;213(6):929-49.
29. Abbasi J. Interest in the Ketogenic Diet Grows for Weight Loss and Type 2 Diabetes. JAMA. 2018;319(3):215-7.
30. Naegele M, Tillack K, Reinhardt S, Schippling S, Martin R, Sospedra M. Neutrophils in multiple sclerosis are characterized by a primed phenotype. Journal of neuroimmunology. 2012;242(1-2):60-71.
31. Wang JX, Bair AM, King SL, Shnayder R, Huang YF, Shieh CC, et al. Ly6G ligation blocks recruitment of neutrophils via a beta2-integrin-dependent mechanism. Blood. 2012;120(7):1489-98.
32. Sas AR, Carbajal KS, Jerome AD, Menon R, Yoon C, Kalinski AL, et al. A new neutrophil subset promotes CNS neuron survival and axon regeneration. Nature immunology. 2020;21(12):1496-505.
33. Ivetic A, Hoskins Green HL, Hart SJ. L-selectin: A Major Regulator of Leukocyte Adhesion, Migration and Signaling. Front Immunol. 2019;10:1068.
34. Ivetic A. A head-to-tail view of L-selectin and its impact on neutrophil behaviour. Cell Tissue Res. 2018;371(3):437-53.
35. Bjorkman L, Christenson K, Davidsson L, Martensson J, Amirbeagi F, Welin A, et al. Neutrophil recruitment to inflamed joints can occur without cellular priming. J Leukoc Biol. 2019;105(6):1123-30.
36. Boer K, Vogelsang H, Deufel T, Pfister W, Kiehntopf M. CD62L on neutrophil granulocytes, a useful, complementary marker for the prediction of ventriculitis in blood-containing CSF. Clin Biochem. 2010;43(16-17):1351-5.
37. Katayama Y, Hidalgo A, Chang J, Peired A, Frenette PS. CD44 is a physiological E-selectin ligand on neutrophils. J Exp Med. 2005;201(8):1183-9.
38. Khan AI, Kerfoot SM, Heit B, Liu L, Andonegui G, Ruffell B, et al. Role of CD44 and hyaluronan in neutrophil recruitment. J Immunol. 2004;173(12):7594-601.
39. Shao Y, Zheng Q, Zhang X, Li P, Gao X, Zhang L, et al. Targeted nuclear degranulation of neutrophils promotes the progression of pneumonia in ulcerative colitis. Precis Clin Med. 2024;7(4):pbae028.
40. Bibi A, Yu Z, Cui L, Yang G. Harnessing monocyte dynamics for treatment of multiple sclerosis; insights from experimental model studies. Immunother Adv. 2025;5(1):ltaf003.
41. Italiani P, Boraschi D. From Monocytes to M1/M2 Macrophages: Phenotypical vs. Functional Differentiation. Front Immunol. 2014;5:514.
42. Novak ML, Koh TJ. Phenotypic transitions of macrophages orchestrate tissue repair. Am J Pathol. 2013;183(5):1352-63.
43. Ramachandran P, Pellicoro A, Vernon MA, Boulter L, Aucott RL, Ali A, et al. Differential Ly-6C expression identifies the recruited macrophage phenotype, which orchestrates the regression of murine liver fibrosis. Proc Natl Acad Sci U S A. 2012;109(46):E3186-95.
44. June CH, Ledbetter JA, Linsley PS, Thompson CB. Role of the CD28 receptor in T-cell activation. Immunol Today. 1990;11(6):211-6.
45. Wetmore E, Lehner-Gulotta D, Florenzo B, Banwell B, Bergqvist AGC, Coleman R, et al. Ketogenic diet in relapsing multiple sclerosis: Patient perceptions, post-trial diet adherence & outcomes. Clin Nutr. 2023;42(8):1427-35.

46. Oh U, Woolbright E, Lehner-Gulotta D, Coleman R, Conaway M, Goldman MD, et al. Serum neurofilament light chain in relapsing multiple sclerosis patients on a ketogenic diet. Mult Scler Relat Disord. 2023;73:104670.
47. Benlloch M, Lopez-Rodriguez MM, Cuerda-Ballester M, Drehmer E, Carrera S, Ceron JJ, et al. Satiating Effect of a Ketogenic Diet and Its Impact on Muscle Improvement and Oxidation State in Multiple Sclerosis Patients. Nutrients. 2019;11(5).
48. Bock M, Karber M, Kuhn H. Ketogenic diets attenuate cyclooxygenase and lipoxygenase gene expression in multiple sclerosis. EBioMedicine. 2018;36:293-303.
49. Choi IY, Piccio L, Childress P, Bollman B, Ghosh A, Brandhorst S, et al. A Diet Mimicking Fasting Promotes Regeneration and Reduces Autoimmunity and Multiple Sclerosis Symptoms. Cell Rep. 2016;15(10):2136-46.
50. Kim DY, Hao J, Liu R, Turner G, Shi FD, Rho JM. Inflammation-mediated memory dysfunction and effects of a ketogenic diet in a murine model of multiple sclerosis. PLoS One. 2012;7(5):e35476.
51. Kim CS, Jung S, Hwang GS, Shin DM. Gut microbiota indole-3-propionic acid mediates neuroprotective effect of probiotic consumption in healthy elderly: A randomized, double-blind, placebo-controlled, multicenter trial and in vitro study. Clin Nutr. 2023;42(6):1025-33.
52. Lin CC, Edelson BT. New Insights into the Role of IL-1beta in Experimental Autoimmune Encephalomyelitis and Multiple Sclerosis. J Immunol. 2017;198(12):4553-60.
53. Pare A, Mailhot B, Levesque SA, Lacroix S. Involvement of the IL-1 system in experimental autoimmune encephalomyelitis and multiple sclerosis: Breaking the vicious cycle between IL-1beta and GM-CSF. Brain, behavior, and immunity. 2017;62:1-8.
54. Savio LEB, de Andrade Mello P, da Silva CG, Coutinho-Silva R. The P2X7 Receptor in Inflammatory Diseases: Angel or Demon? Front Pharmacol. 2018;9:52.
55. Sun W, Wang Q, Zhang R, Zhang N. Ketogenic diet attenuates neuroinflammation and induces conversion of M1 microglia to M2 in an EAE model of multiple sclerosis by regulating the NF-kappaB/NLRP3 pathway and inhibiting HDAC3 and P2X7R activation. Food Funct. 2023;14(15):7247-69.
56. Digby JE, Martinez F, Jefferson A, Ruparelia N, Chai J, Wamil M, et al. Anti-inflammatory effects of nicotinic acid in human monocytes are mediated by GPR109A dependent mechanisms. Arterioscler Thromb Vasc Biol. 2012;32(3):669-76.
57. Lukasova M, Malaval C, Gille A, Kero J, Offermanns S. Nicotinic acid inhibits progression of atherosclerosis in mice through its receptor GPR109A expressed by immune cells. J Clin Invest. 2011;121(3):1163-73.
58. Zandi-Nejad K, Takakura A, Jurewicz M, Chandraker AK, Offermanns S, Mount D, et al. The role of HCA2 (GPR109A) in regulating macrophage function. FASEB J. 2013;27(11):4366-74.
59. Chen H, Assmann JC, Krenz A, Rahman M, Grimm M, Karsten CM, et al. Hydroxycarboxylic acid receptor 2 mediates dimethyl fumarate's protective effect in EAE. J Clin Invest. 2014;124(5):2188-92.
60. Rahman M, Muhammad S, Khan MA, Chen H, Ridder DA, Muller-Fielitz H, et al. The beta-hydroxybutyrate receptor HCA2 activates a neuroprotective subset of macrophages. Nature communications. 2014;5:3944.
61. Li R, Liu Y, Wu J, Chen X, Lu Q, Xia K, et al. Adaptive Metabolic Responses Facilitate Blood-Brain Barrier Repair in Ischemic Stroke via BHB-Mediated Epigenetic Modification of ZO-1 Expression. Adv Sci (Weinh). 2024;11(25):e2400426.
62. Wang Z, Li T, Du M, Zhang L, Xu L, Song H, et al. beta-hydroxybutyrate improves cognitive impairment caused by chronic cerebral hypoperfusion via amelioration of neuroinflammation and blood-brain barrier damage. Brain Res Bull. 2023;193:117-30.
63. Li B, Yu Y, Liu K, Zhang Y, Geng Q, Zhang F, et al. beta-Hydroxybutyrate inhibits histone deacetylase 3 to promote claudin-5 generation and attenuate cardiac microvascular hyperpermeability in diabetes. Diabetologia. 2021;64(1):226-39.
64. Lu H, Ashiqueali R, Lin CI, Walchale A, Clendaniel V, Matheson R, et al. Histone Deacetylase 3 Inhibition Decreases Cerebral Edema and Protects the Blood-Brain Barrier After Stroke. Mol Neurobiol. 2023;60(1):235-46.
65. Tan K, Rodriguez-Fernandez MM, Keuler T, Hansen FK, Gutschow M, Weindl G, et al. Crosstalk between NLRP3 Signaling and Histone Deacetylases in Inflammasome-Driven Diseases. Journal of medicinal chemistry. 2026;69(1):102-20.

66. Openshaw H, Stuve O, Antel JP, Nash R, Lund BT, Weiner LP, et al. Multiple sclerosis flares associated with recombinant granulocyte colony-stimulating factor. Neurology. 2000;54(11):2147-50.
67. Steinbach K, Piedavent M, Bauer S, Neumann JT, Friese MA. Neutrophils amplify autoimmune central nervous system infiltrates by maturing local APCs. J Immunol. 2013;191(9):4531-9.
68. Wang Y, Jin S, Sonobe Y, Cheng Y, Horiuchi H, Parajuli B, et al. Interleukin-1beta induces blood-brain barrier disruption by downregulating Sonic hedgehog in astrocytes. PLoS One. 2014;9(10):e110024.
69. Yoon SH, Kim CY, Lee E, Lee C, Lee KS, Lee J, et al. Microglial NLRP3-gasdermin D activation impairs blood-brain barrier integrity through interleukin-1beta-independent neutrophil chemotaxis upon peripheral inflammation in mice. Nature communications. 2025;16(1):699.
70. Wei C, Jiang W, Wang R, Zhong H, He H, Gao X, et al. Brain endothelial GSDMD activation mediates inflammatory BBB breakdown. Nature. 2024;629(8013):893-900.
71. Xu Y, Chen Y, Zhang X, Ma J, Liu Y, Cui L, et al. Glycolysis in Innate Immune Cells Contributes to Autoimmunity. Front Immunol. 2022;13:920029.
72. Walmsley SR, Print C, Farahi N, Peyssonnaux C, Johnson RS, Cramer T, et al. Hypoxia-induced neutrophil survival is mediated by HIF-1alpha-dependent NF-kappaB activity. J Exp Med. 2005;201(1):105-15.
73. Jun HS, Lee YM, Song KD, Mansfield BC, Chou JY. G-CSF improves murine G6PC3-deficient neutrophil function by modulating apoptosis and energy homeostasis. Blood. 2011;117(14):3881-92.
74. Kim ER, Kim SR, Cho W, Lee SG, Kim SH, Kim JH, et al. Short Term Isocaloric Ketogenic Diet Modulates NLRP3 Inflammasome Via B-hydroxybutyrate and Fibroblast Growth Factor 21. Front Immunol. 2022;13:843520.
75. Kong G, Wang J, Li R, Huang Z, Wang L. Ketogenic diet ameliorates inflammation by inhibiting the NLRP3 inflammasome in osteoarthritis. Arthritis Res Ther. 2022;24(1):113.
76. Parveen K, Salman M, Mirzahosseini G, Parveen A, Ishrat T, Puchowicz MA. Chronic Ketosis Provides Neuroprotection Through HIF- 1alpha-Mediated Control of the TXNIP/NLRP3 Axis by Regulating the Inflammatory and Apoptotic Response. Mol Neurobiol. 2025;62(9):11238-52.
77. Youm YH, Nguyen KY, Grant RW, Goldberg EL, Bodogai M, Kim D, et al. The ketone metabolite beta-hydroxybutyrate blocks NLRP3 inflammasome-mediated inflammatory disease. Nat Med. 2015;21(3):263-9.
78. Lee J, Cho W, Yu JW, Hyun YM. NLRP3 activation induces BBB disruption and neutrophil infiltration via CXCR2 signaling in the mouse brain. Journal of neuroinflammation. 2025;22(1):139.
79. Na YR, Gu GJ, Jung D, Kim YW, Na J, Woo JS, et al. GM-CSF Induces Inflammatory Macrophages by Regulating Glycolysis and Lipid Metabolism. J Immunol. 2016;197(10):4101-9.
80. Purvis GSD, McNeill E, Wright B, Channon KM, Greaves DR. Ly6C(hi) Monocytes Are Metabolically Reprogrammed in the Blood during Inflammatory Stimulation and Require Intact OxPhos for Chemotaxis and Monocyte to Macrophage Differentiation. Cells. 2024;13(11).
81. Fani Maleki A, Cisbani G, Laflamme N, Prefontaine P, Plante MM, Baillargeon J, et al. Selective Immunomodulatory and Neuroprotective Effects of a NOD2 Receptor Agonist on Mouse Models of Multiple Sclerosis. Neurotherapeutics. 2021;18(2):889-904.
82. Forde EA, Dogan RN, Karpus WJ. CCR4 contributes to the pathogenesis of experimental autoimmune encephalomyelitis by regulating inflammatory macrophage function. Journal of neuroimmunology. 2011;236(1-2):17-26.
83. Zimmermann J, Nitsch L, Krauthausen M, Muller M. IL-17A Facilitates Entry of Autoreactive T-Cells and Granulocytes into the CNS During EAE. Neuromolecular Med. 2023;25(3):350-9.
84. Desli E, Spilioti M, Evangeliou A, Styllas F, Magkos F, Dalamaga M. The Efficacy and Safety of Ketogenic Diets in Drug-Resistant Epilepsy in Children and Adolescents: a Systematic Review of Randomized Controlled Trials. Curr Nutr Rep. 2022;11(2):102-16.
85. Phillips MCL, Johnston SE, Simpson P, Chang DK, Mather D, Dick RJ. Time-restricted ketogenic diet in amyotrophic lateral sclerosis: a case study. Frontiers in neurology. 2023;14:1329541.
86. Rusek M, Pluta R, Ulamek-Koziol M, Czuczwar SJ. Ketogenic Diet in Alzheimer's Disease. International journal of molecular sciences. 2019;20(16).

87. Sethi S, Wakeham D, Ketter T, Hooshmand F, Bjornstad J, Richards B, et al. Ketogenic Diet Intervention on Metabolic and Psychiatric Health in Bipolar and Schizophrenia: A Pilot Trial. Psychiatry Res. 2024;335:115866.
88. Tidman MM, White DR, White TA. Impact of a keto diet on symptoms of Parkinson's disease, biomarkers, depression, anxiety and quality of life: a longitudinal study. Neurodegener Dis Manag. 2024;14(3-4):97-110.
89. Leavy O. Regulatory T cells: Going over to the dark side. Nat Rev Immunol. 2014;14(1):5.
90. Price AE, Reinhardt RL, Liang HE, Locksley RM. Marking and quantifying IL-17A-producing cells in vivo. PLoS One. 2012;7(6):e39750.

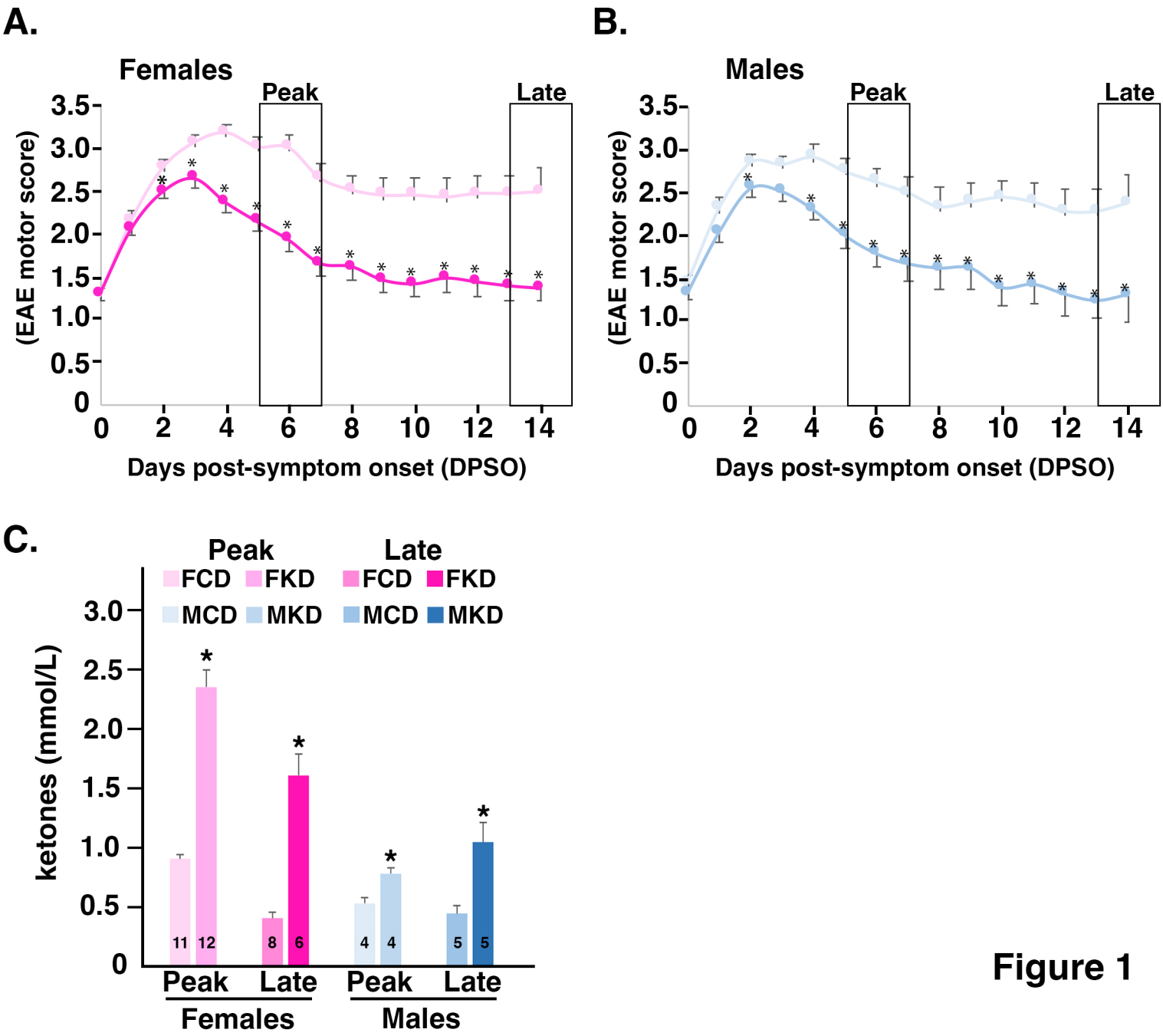
A.
Females
Peak
Late
(EAE motor score)
Days post-symptom onset (DPSO)
B.
Males
Peak
Late
(EAE motor score)
Days post-symptom onset (DPSO)
C.
Peak
Late
FCD
FKD
FCD
FKD
MCD
MKD
MCD
MKD
ketones (mmol/L)
11
12
8
6
4
4
5
5
Peak
Late
Peak
Late
Females
Males

Figure 1

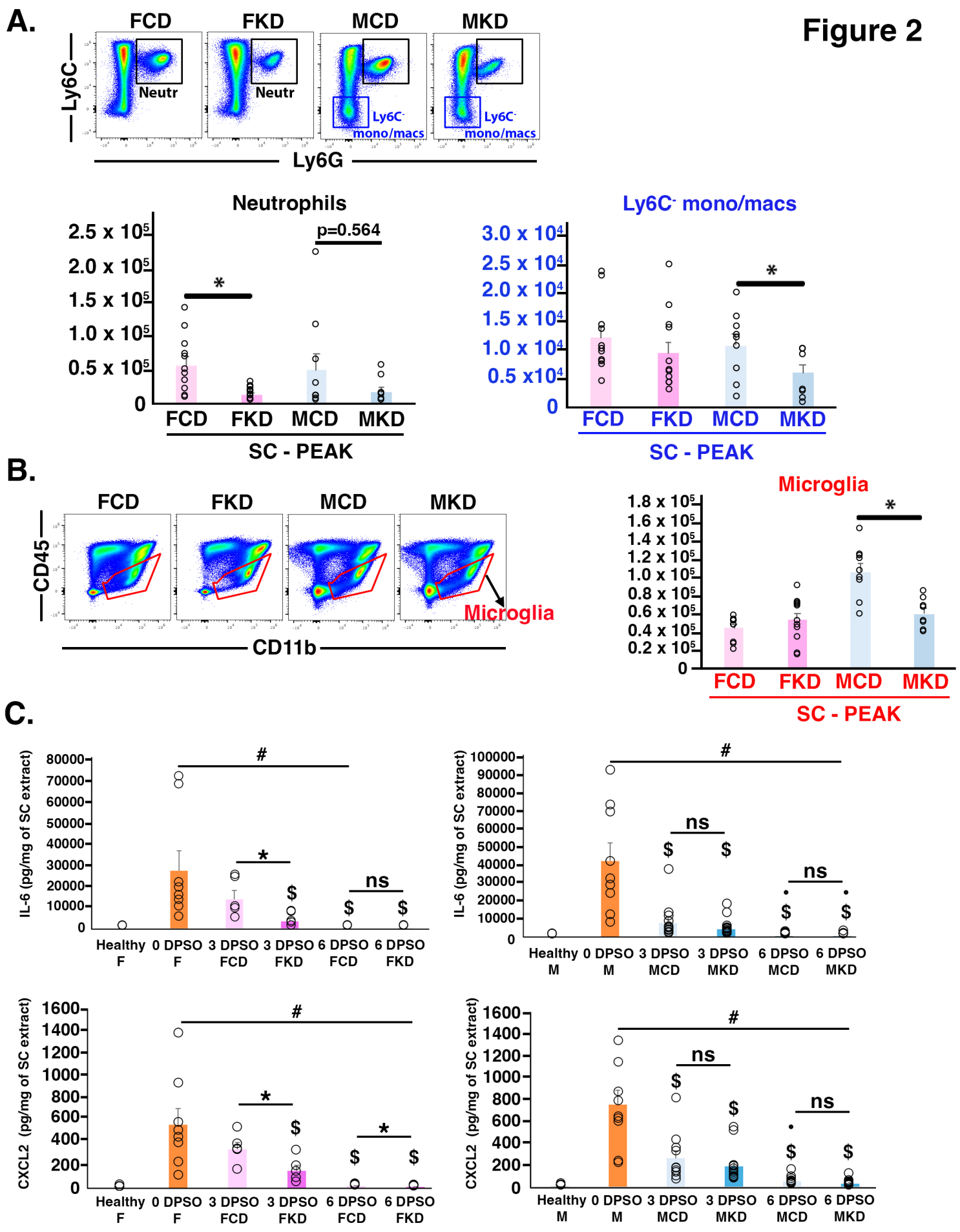
Figure 2
A.
FCD
FKD
MCD
MKD
Ly6C
Ly6G
Neutr
Ly6C-
mono/macs
Neutrophils
p=0.564
SC - PEAK
Ly6C- mono/macs
B.
CD45
CD11b
Microglia
C.
IL-6 (pg/mg of SC extract)
CXCL2 (pg/mg of SC extract)
Healthy F
0 DPSO F
3 DPSO FCD
3 DPSO FKD
6 DPSO FCD
6 DPSO FKD
Healthy M
0 DPSO M
3 DPSO MCD
3 DPSO MKD
6 DPSO MCD
6 DPSO MKD
ns

Figure 2

D.

SC - LATE

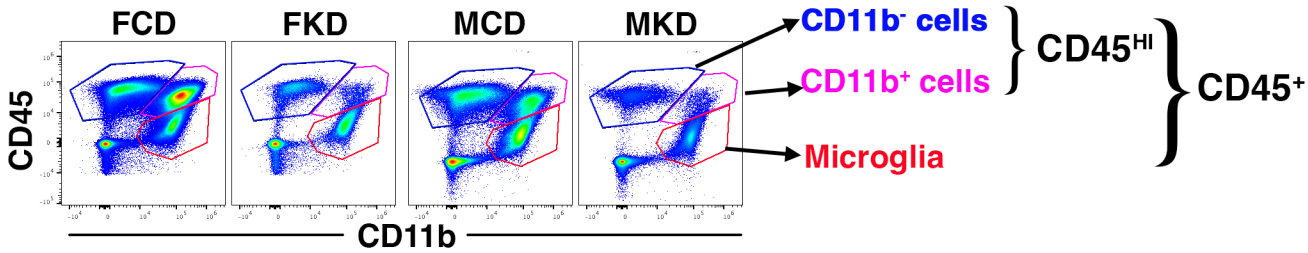

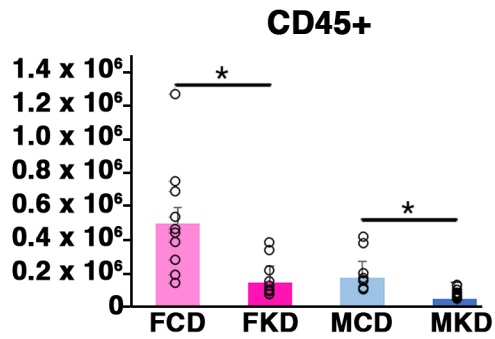

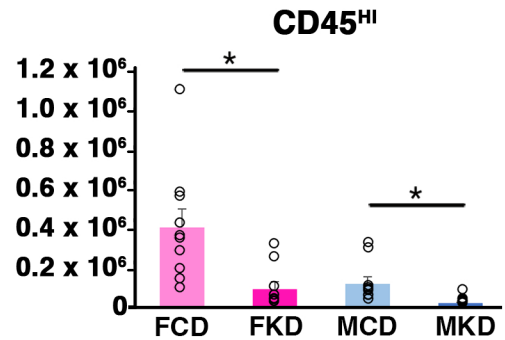

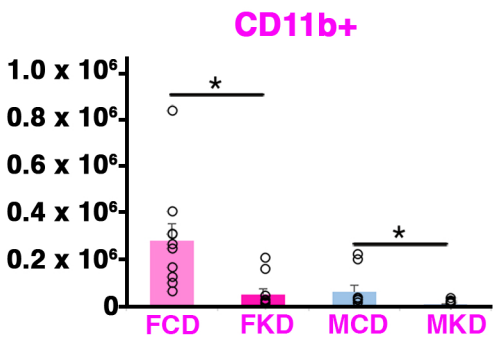

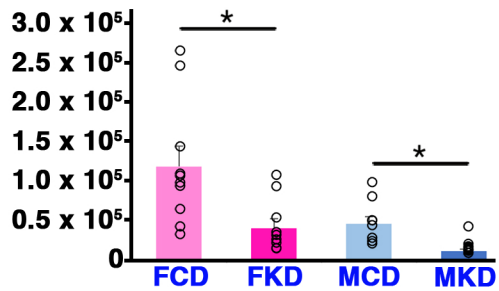

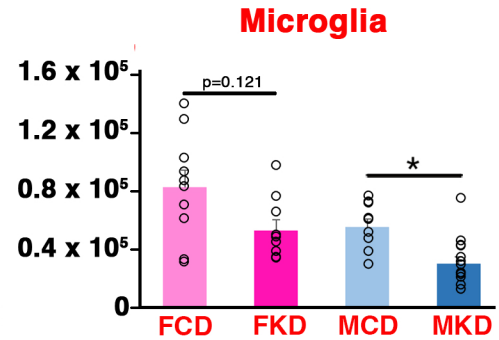

E.

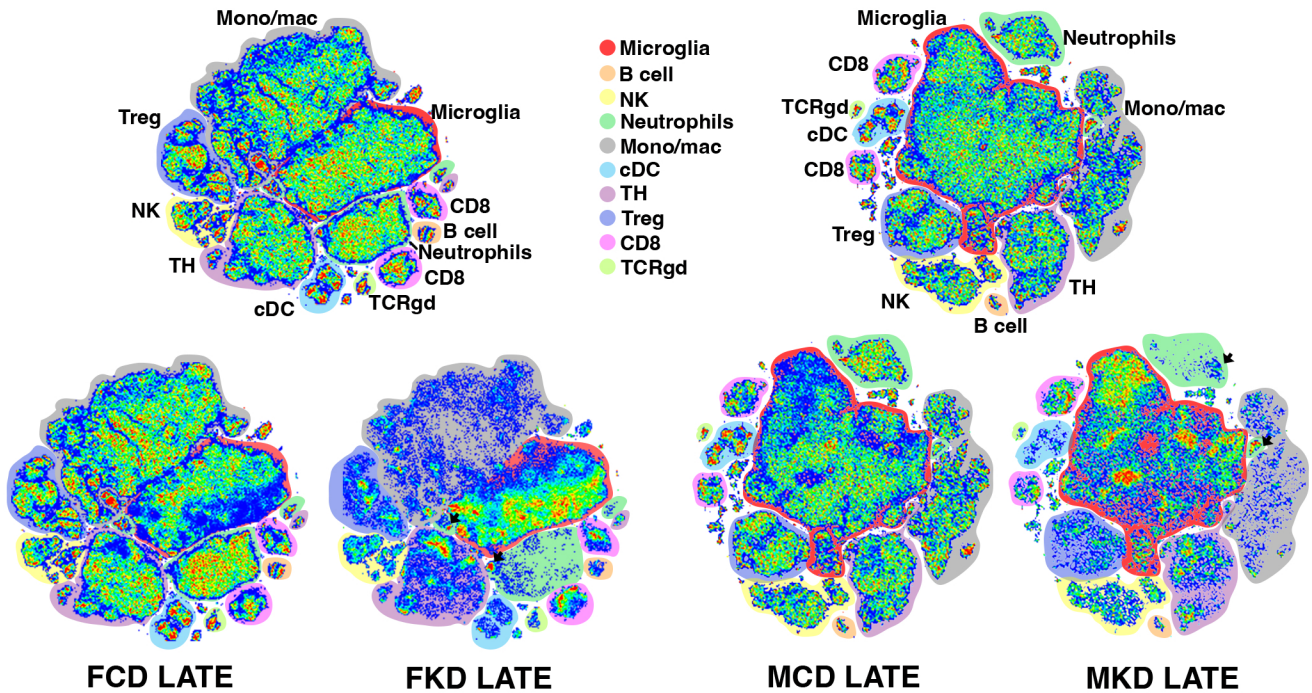

Figure 2

F.

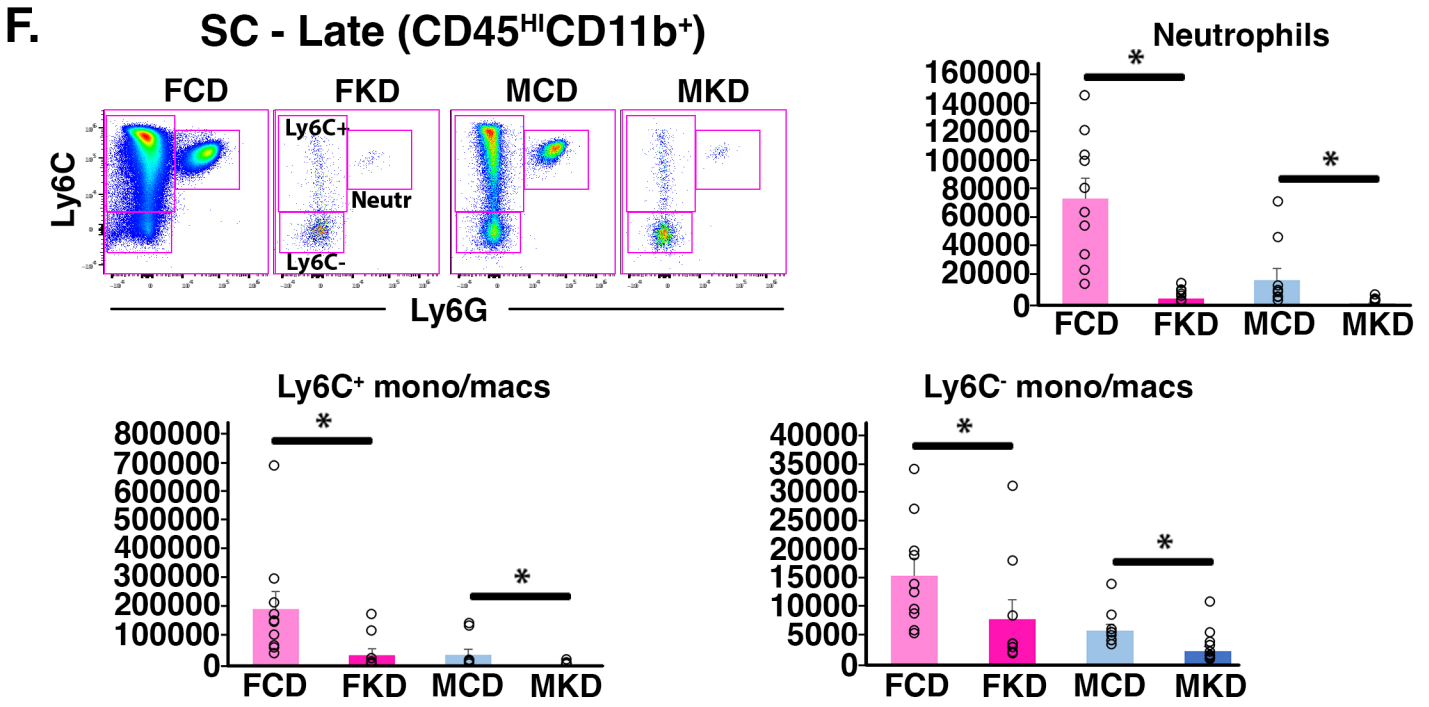
SC - Late (CD45HICD11b+)
FCD
FKD
MCD
MKD
Ly6C
Ly6G
Ly6C+
Neutr
Ly6C-
Neutrophils
160000
140000
120000
100000
80000
60000
40000
20000
0
*
Ly6C+ mono/macs
800000
700000
600000
500000
400000
300000
200000
100000
Ly6C- mono/macs
40000
35000
30000
25000
20000
15000
10000
5000

G.

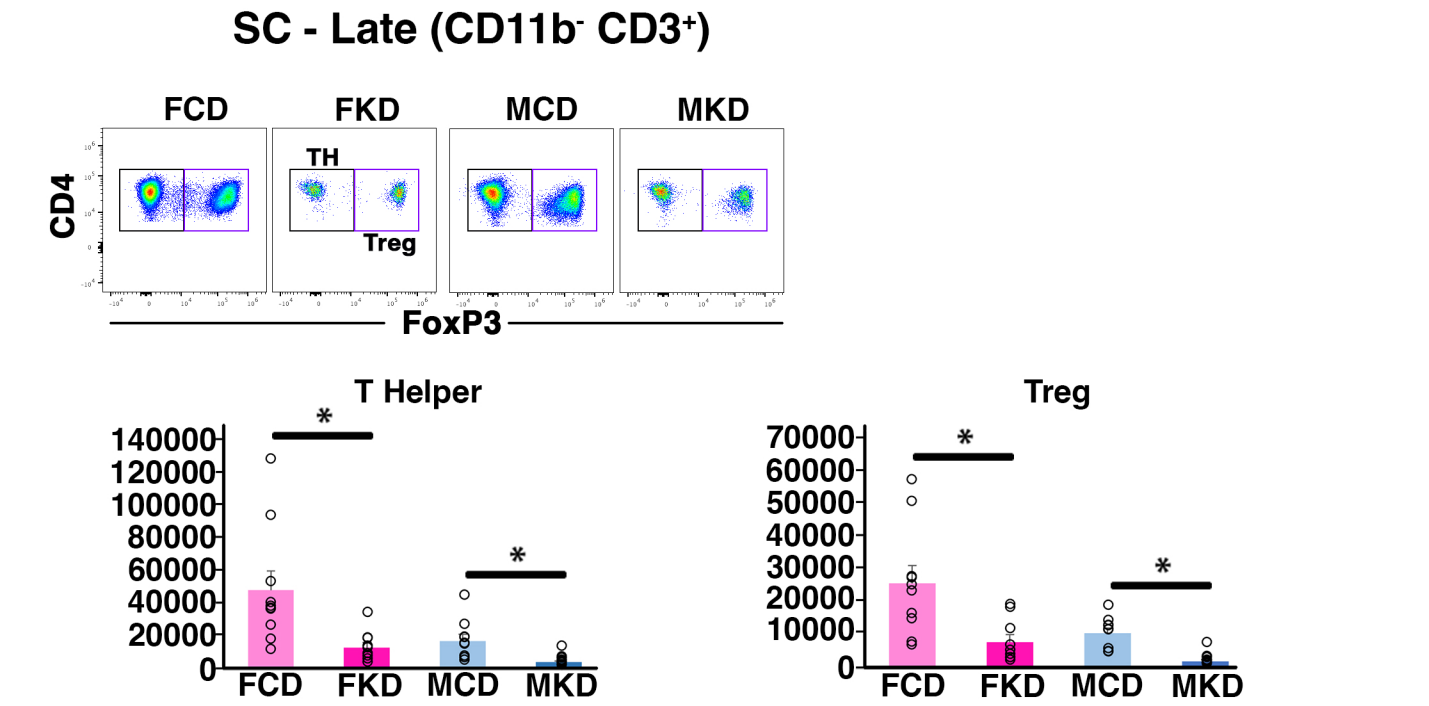
SC - Late (CD11b- CD3+)
FCD
FKD
MCD
MKD
CD4
FoxP3
TH
Treg
T Helper
140000
120000
100000
80000
60000
40000
20000
0
*
Treg
70000
60000
50000
40000
30000
20000
10000

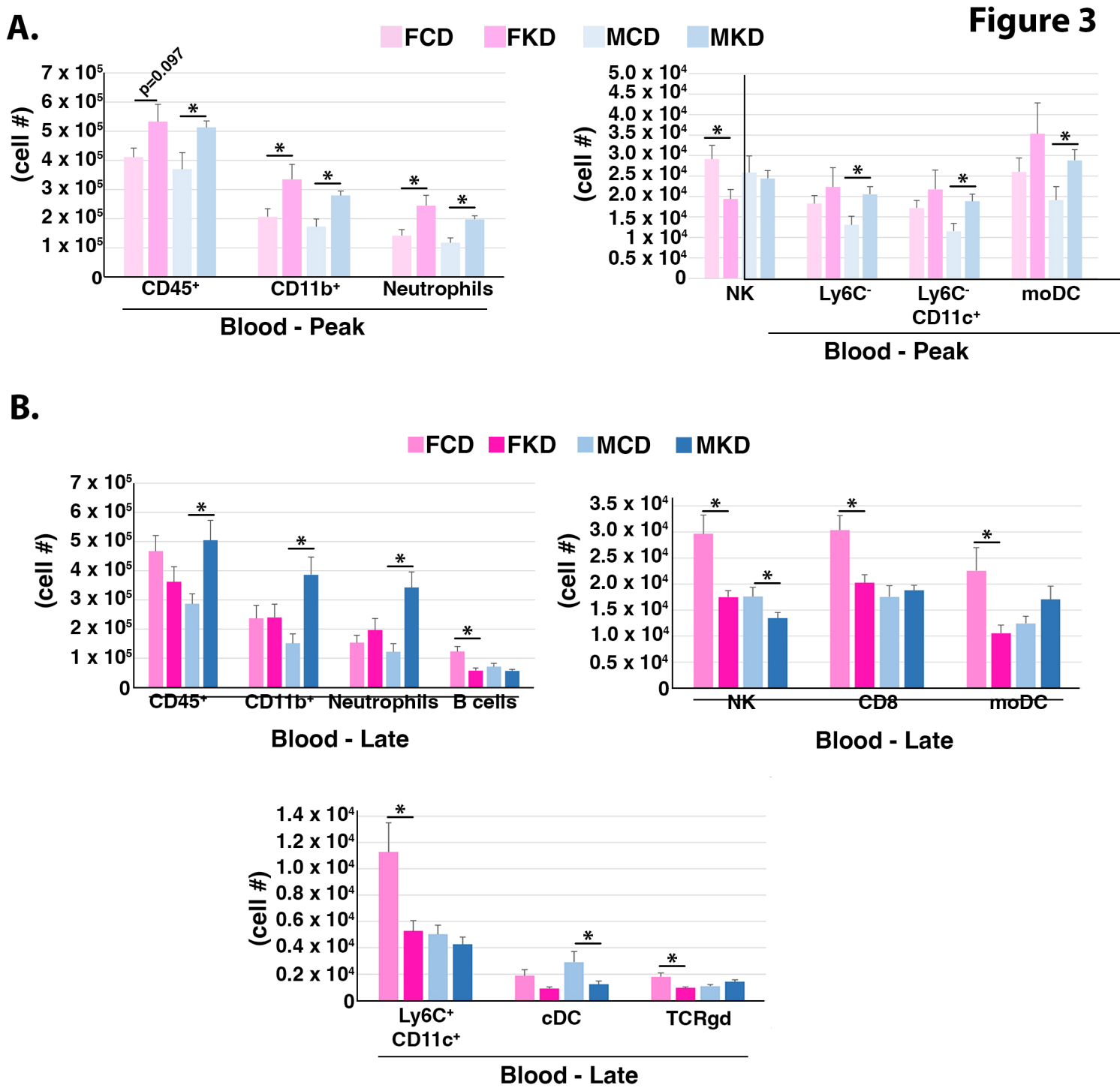
Figure 3
A.
FCD
FKD
MCD
MKD
(cell #)
7 x 10^5
6 x 10^5
5 x 10^5
4 x 10^5
3 x 10^5
2 x 10^5
1 x 10^5
0
p=0.097
*
CD45+
CD11b+
Neutrophils
Blood - Peak
5.0 x 10^4
4.5 x 10^4
4.0 x 10^4
3.5 x 10^4
3.0 x 10^4
2.5 x 10^4
2.0 x 10^4
1.5 x 10^4
1 x 10^4
0.5 x 10^4
NK
Ly6C-
Ly6C- CD11c+
moDC
Blood - Peak
B.
FCD
FKD
MCD
MKD
CD45+
CD11b+
Neutrophils
B cells
Blood - Late
3.5 x 10^4
3.0 x 10^4
2.5 x 10^4
2.0 x 10^4
1.5 x 10^4
1.0 x 10^4
0.5 x 10^4
NK
CD8
moDC
Blood - Late
1.4 x 10^4
1.2 x 10^4
1.0 x 10^4
0.8 x 10^4
0.6 x 10^4
0.4 x 10^4
0.2 x 10^4
Ly6C+ CD11c+
cDC
TCRgd
Blood - Late

Figure 4

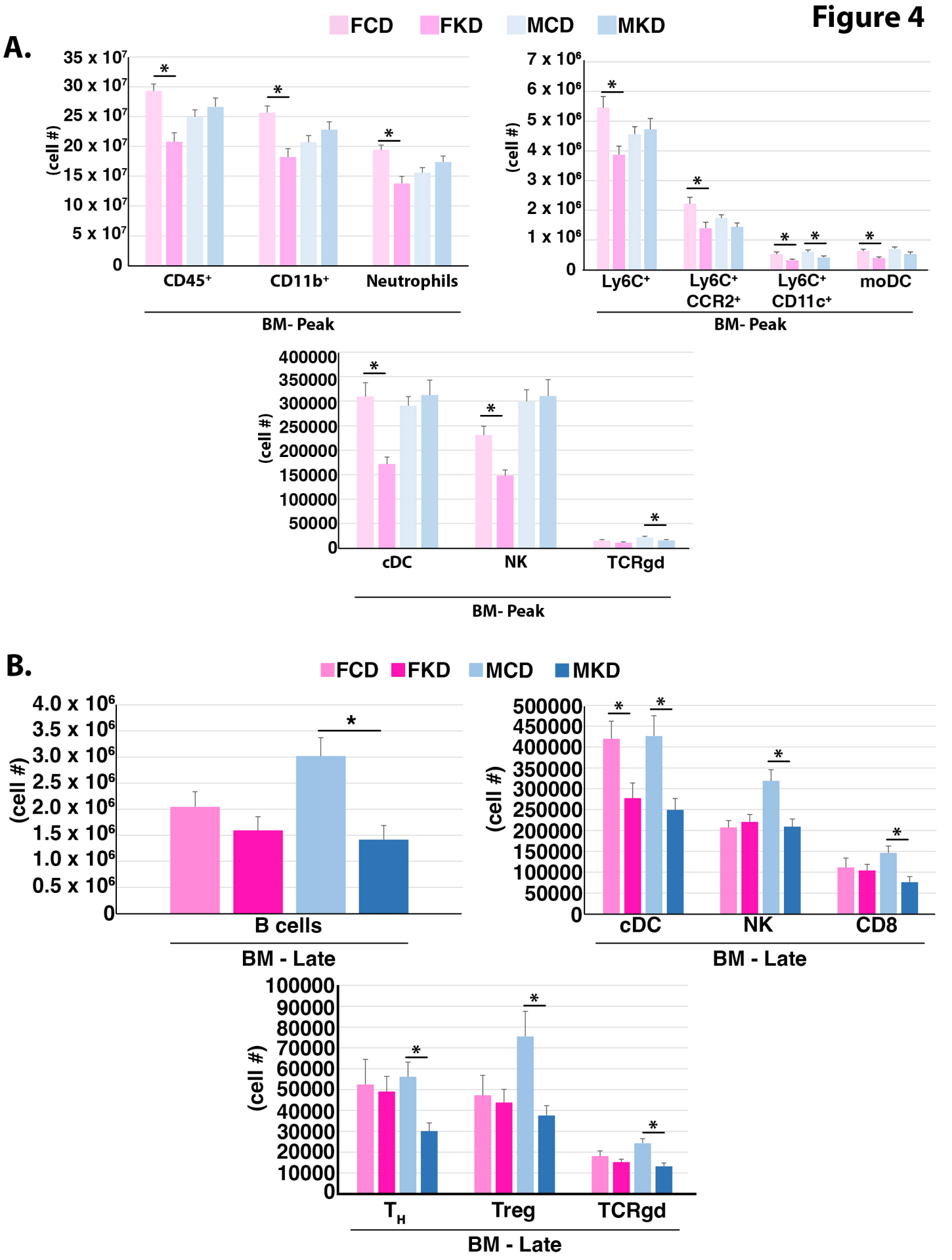
A.
FCD
FKD
MCD
MKD
(cell #)
35 x 10^7
30 x 10^7
25 x 10^7
20 x 10^7
15 x 10^7
10 x 10^7
5 x 10^7
0
CD45+
CD11b+
Neutrophils
BM- Peak
7 x 10^6
6 x 10^6
5 x 10^6
4 x 10^6
3 x 10^6
2 x 10^6
1 x 10^6
Ly6C+
Ly6C+ CCR2+
Ly6C+ CD11c+
moDC
400000
350000
300000
250000
200000
150000
100000
50000
cDC
NK
TCRgd
B.
4.0 x 10^6
3.5 x 10^6
3.0 x 10^6
2.5 x 10^6
2.0 x 10^6
1.5 x 10^6
1.0 x 10^6
0.5 x 10^6
B cells
BM - Late
500000
450000
400000
350000
300000
250000
200000
150000
100000
50000
CD8
100000
90000
80000
70000
60000
50000
40000
30000
20000
10000
T_H
Treg

Figure 5

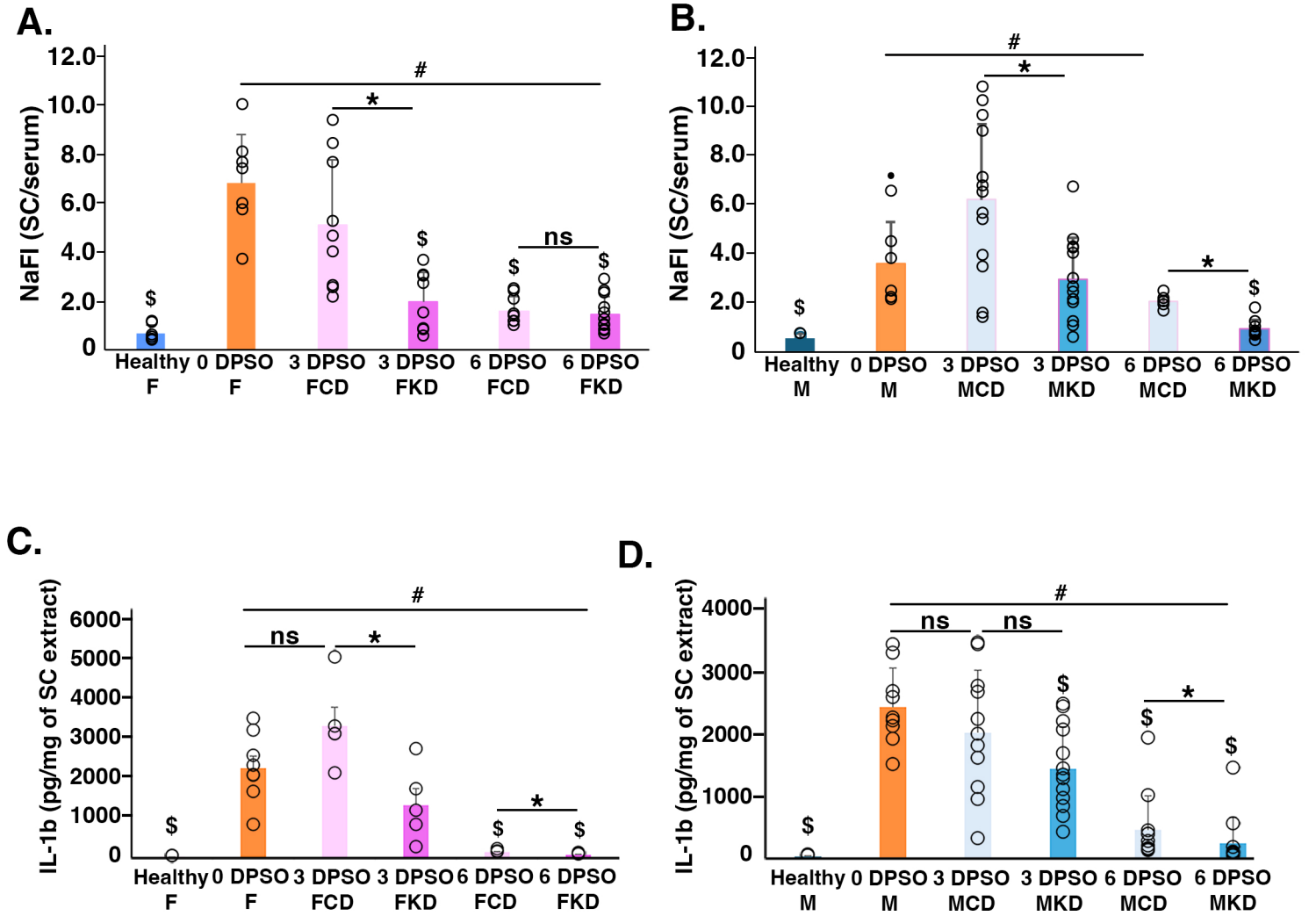
A.
NaFI (SC/serum)
12.0
10.0
8.0
6.0
4.0
2.0
0
#
*
ns
$
Healthy F
0 DPSO F
3 DPSO FCD
3 DPSO FKD
6 DPSO FCD
6 DPSO FKD
B.
NaFI (SC/serum)
Healthy M
0 DPSO M
3 DPSO MCD
3 DPSO MKD
6 DPSO MCD
6 DPSO MKD
C.
IL-1b (pg/mg of SC extract)
6000
5000
4000
3000
2000
1000
0
D.
IL-1b (pg/mg of SC extract)
4000
3000
2000
1000
0

Figure 6

A.

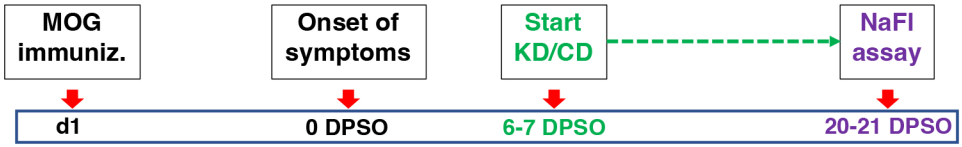

B.

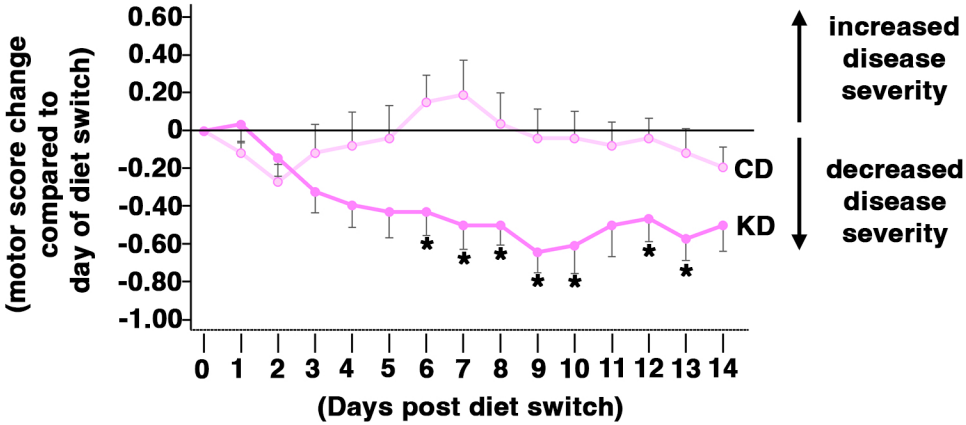

C.

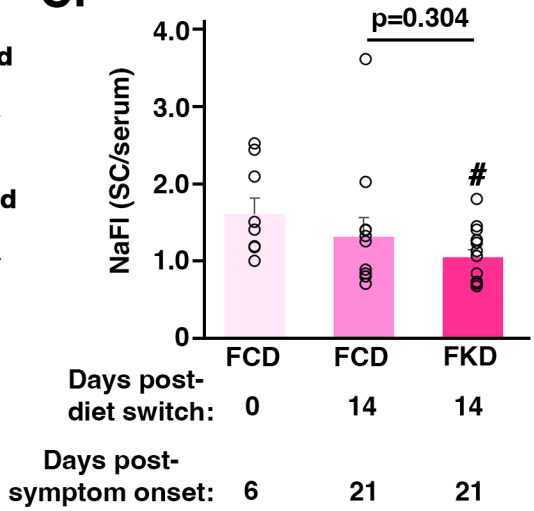

D.

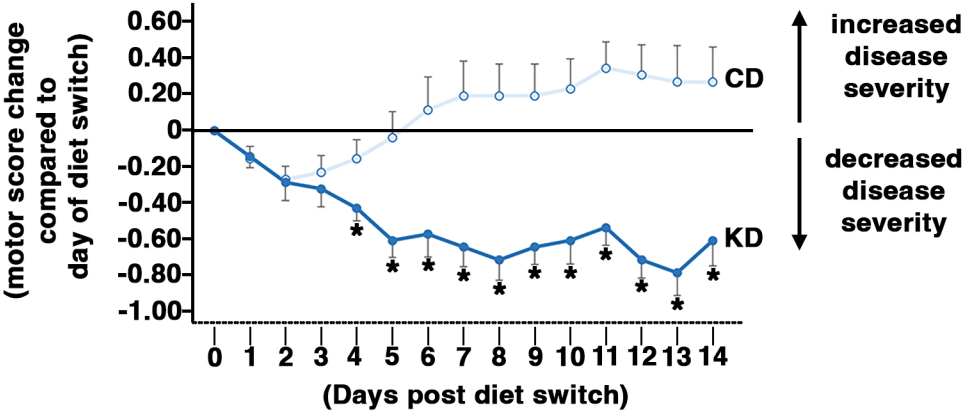

E.

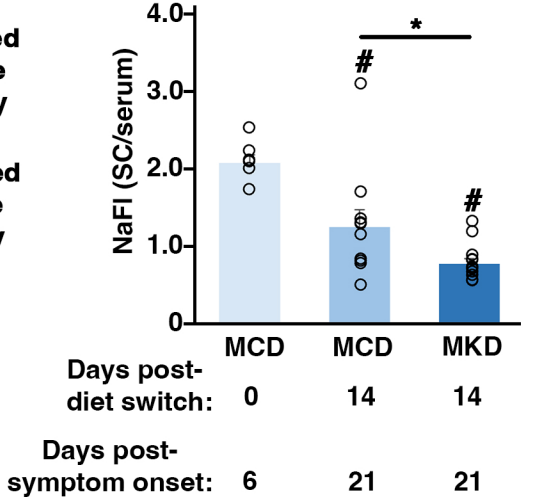

Figure 7

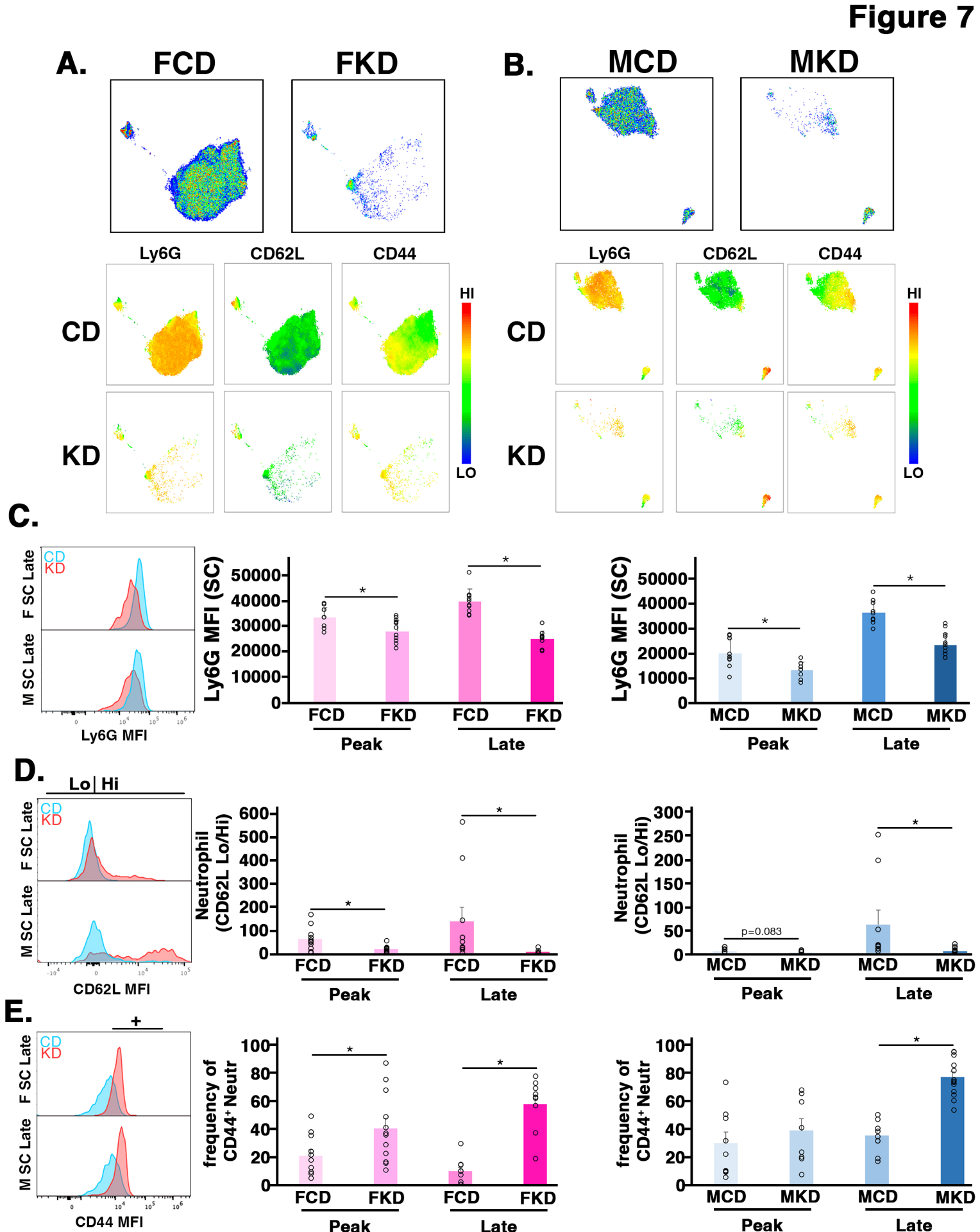
A.
FCD
FKD
B.
MCD
MKD
Ly6G
CD62L
CD44
CD
KD
HI
LO
C.
CD
KD
F SC Late
M SC Late
Ly6G MFI
Ly6G MFI (SC)
FCD
FKD
MCD
MKD
Peak
Late
D.
Lo| Hi
CD62L MFI
Neutrophil (CD62L Lo/Hi)
p=0.083
E.
+
CD44 MFI
frequency of CD44+ Neutr

Figure 8

A.

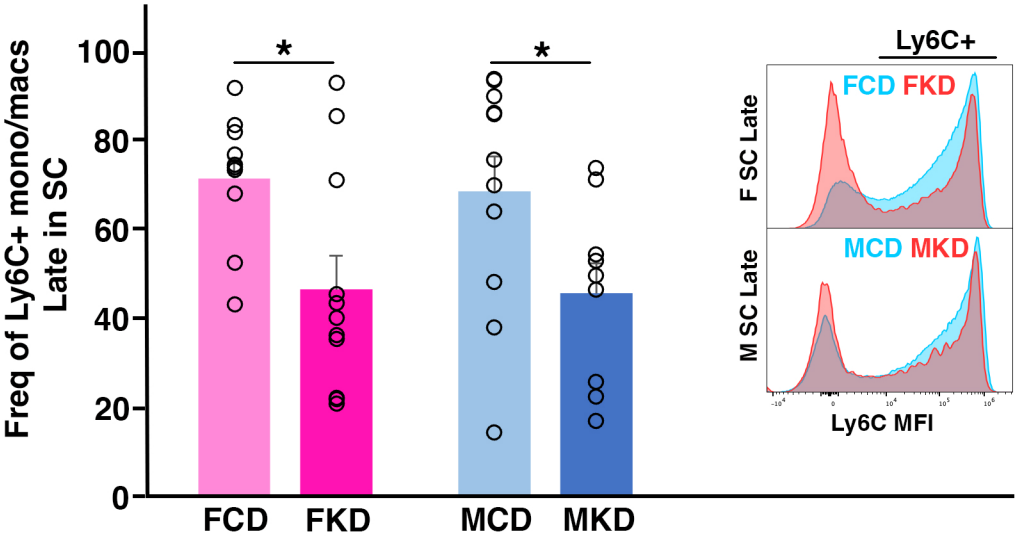
Freq of Ly6C+ mono/macs Late in SC
100
80
60
40
20
0
*
*
FCD
FKD
MCD
MKD
Ly6C+
FCD FKD
F SC Late
MCD MKD
M SC Late
Ly6C MFI

B.

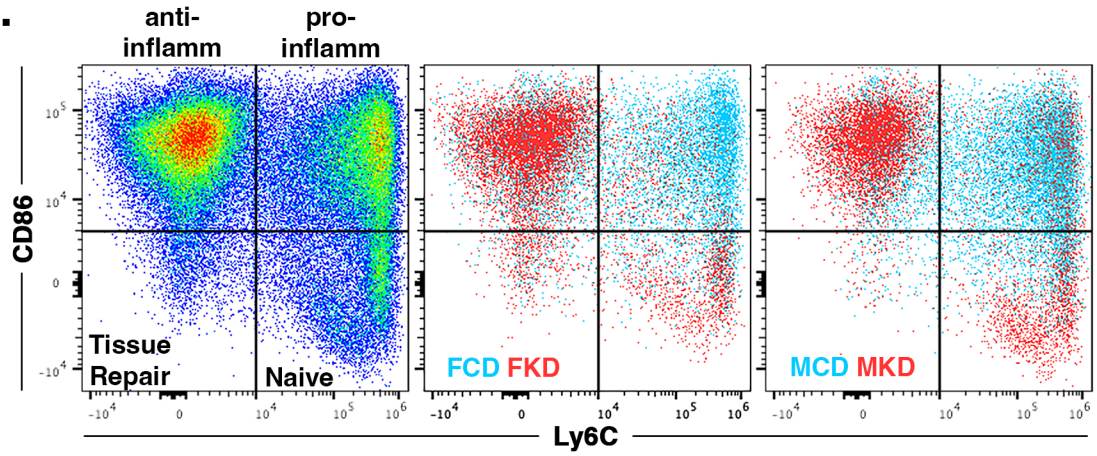
anti-inflamm
pro-inflamm
CD86
Tissue Repair
Naive
FCD FKD
MCD MKD
Ly6C

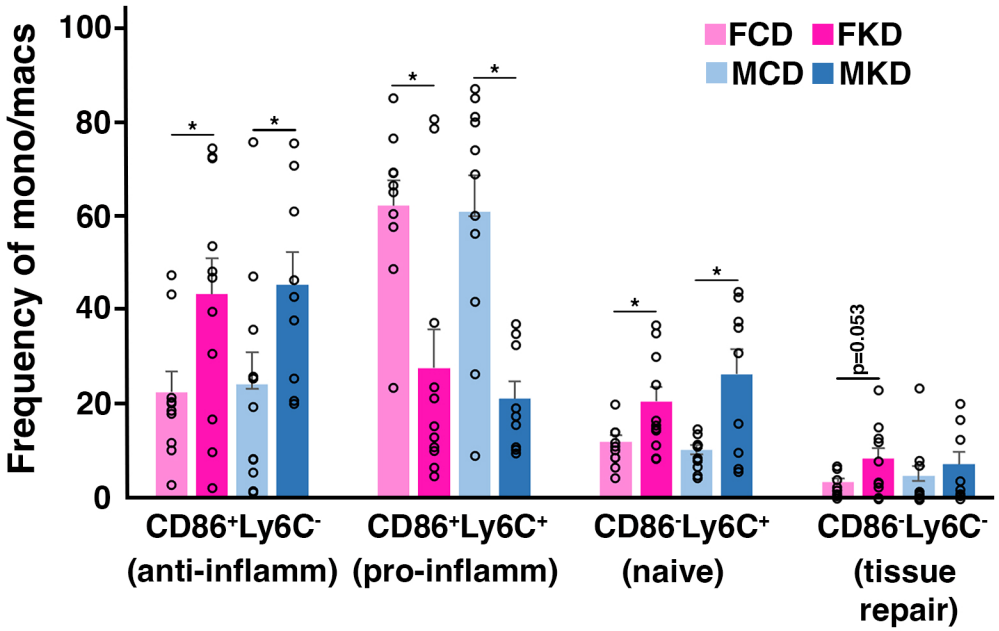
Frequency of mono/macs
100
80
60
40
20
0
FCD
FKD
MCD
MKD
*
*
*
*
*
*
p=0.053
CD86+Ly6C- (anti-inflamm)
CD86+Ly6C+ (pro-inflamm)
CD86-Ly6C+ (naive)
CD86-Ly6C- (tissue repair)

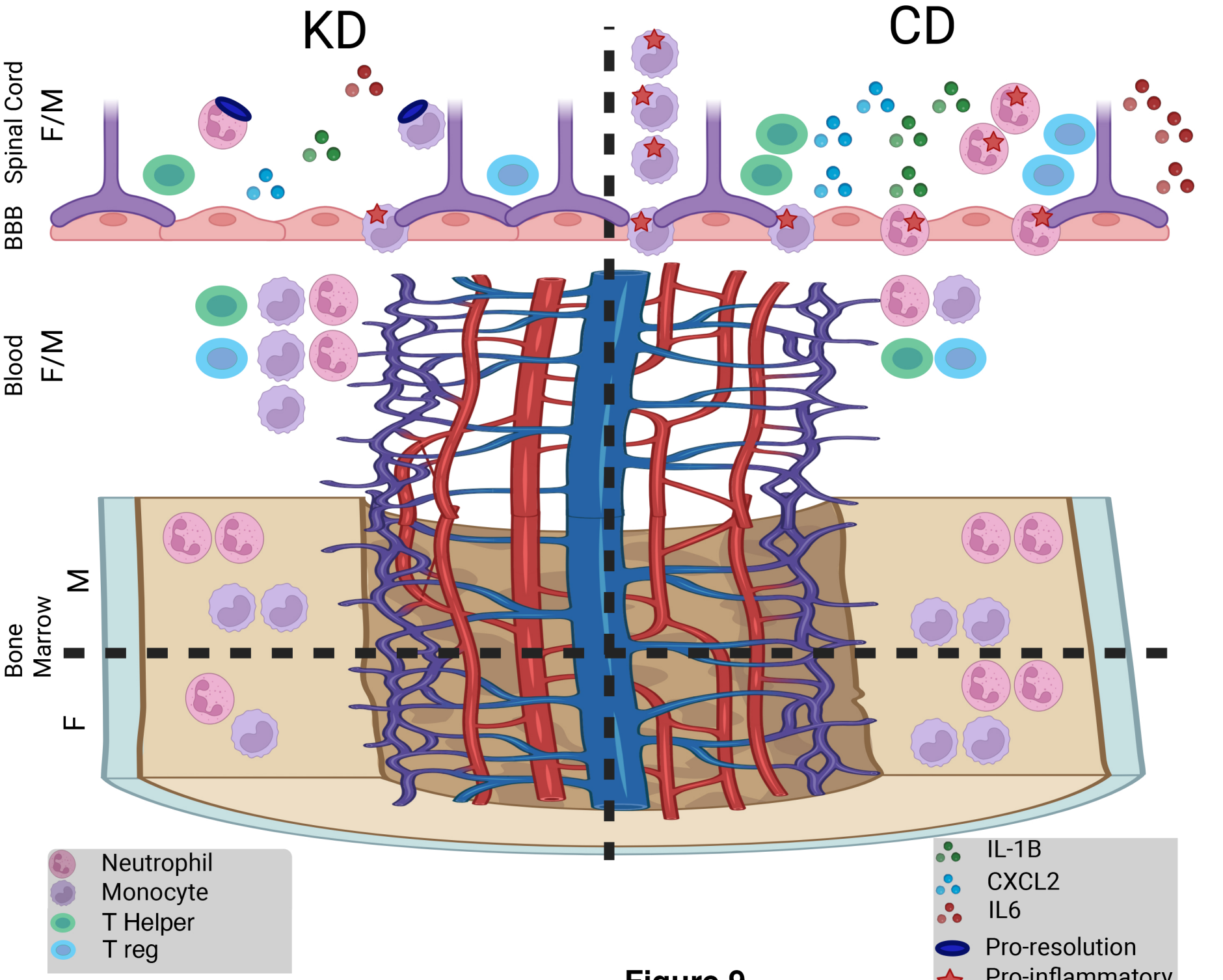
KD
CD
Spinal Cord
F/M
BBB
Blood
F/M
Bone
Marrow
M
F
Neutrophil
Monocyte
T Helper
T reg
IL-1B
CXCL2
IL6
Pro-resolution
Pro-inflammatory

Figure 9

Table 1

	FOLD CHNG v CD*		FOLD CHNG v CD**		FOLD CHNG v CD**	
	SC PEAK FKD	SC PEAK MKD	Blood PEAK FKD	Blood PEAK MKD	BM PEAK FKD	BM PEAK MKD
CD45hi			NA	NA	NA	NA
CD45+				1.39	0.71	
Bcells						
NK			0.67		0.64	
NKT						
CD11b+			1.62	1.62	0.71	
Neutr	0.24		1.73	1.67	0.71	
Ly6C-		0.55		1.57		
Ly6C-CCR2+						
Ly6C-CD11c+				1.63		
Ly6C+					0.71	
Ly6C+ CCR2+					0.63	
Ly6C+ CD11c+					0.61	0.68
moDC				1.51	0.63	
cDC					0.55	
TH						
Treg						
CD8						
TCRgd						0.74
Microglia		0.57				
Mono						
Ly6C+Mono						
Ly6C-Mono						
Mac						
Ly6C+Mac						
Ly6C-Mac						

*Shapiro-Wilk test

*Mann-Whitney U Test

**2-tailed, unpaired Student's t-test

KD/CD FOLD CHNG
3.00
2.00
1.50
1.00
0.75
0.50
0.25
0.00

Table 2

	FOLD CHNG v CD*		FOLD CHNG v CD**				FOLD CHNG v CD**			
	SC LATE FKD	SC LATE MKD	Blood LATE FKD	Blood Healthy FKD	Blood LATE MKD	Blood Healthy MKD	BM LATE FKD	BM Healthy FKD	BM LATE MKD	BM Healthy MKD
CD45hi	0.23	0.17	NA	NA	NA	NA	NA	NA	NA	NA
CD45+	0.30	0.29			1.76	1.60				1.25
Bcells		0.27	0.47						0.47	0.54
NK	0.31	0.22	0.59	0.64	0.76				0.66	
NKT	0.19	0.31								
CD11b+	0.17	0.10			2.55	2.86				1.47
Neutr	0.06	0.06			2.82	3.35				1.53
Ly6C-	0.51	0.40		0.72						
Ly6C-CCR2+	0.31	0.22				2.38				0.59
Ly6C-CD11c+	0.53	0.45				1.39		0.58		
Ly6C+	0.19	0.07		0.53		1.74				1.35
Ly6C+ CCR2+	0.20	0.07		0.57		1.88				1.39
Ly6C+ CD11c	0.25	0.11	0.47	0.57						
moDC	0.29	0.20		0.67		1.62				
cDC	0.40	0.14		0.35	0.42		0.66		0.58	0.79
TH	0.27	0.24							0.54	0.47
Treg	0.30	0.18							0.50	0.56
CD8		0.45	0.67	0.81					0.52	0.50
TCRgd	0.66	0.28	0.53	0.63					0.55	0.54
Microglia		0.54	*Shapiro-Wilk test							
Mono	0.16	0.11	*Mann-Whitney U Test							
Ly6C+Mono	0.09	0.09								
Ly6C-Mono	0.54	0.16	**2-tailed, unpaired Student's t-test							
Mac	0.23	0.12								
Ly6C+Mac	0.22	0.07								
Ly6C-Mac	0.45	0.64								

KD/CD FOLD CHNG
3.00
2.00
1.50
1.00
0.75
0.50
0.25
0.00